JCB

Brr6 and Brl1 locate to nuclear pore complex assembly sites to promote their biogenesis

Wanlu Zhang,[1] Annett Neuner,[1] Diana Rüthnick,[1] Timo Sachsenheimer,[2] Christian Lüchtenborg,[2] Britta Brügger,[2] and Elmar Schiebel[1]

[1]Zentrum für Molekulare Biologie der Universität Heidelberg, DKFZ-ZMBH Allianz, Heidelberg, Germany
[2]Heidelberg University Biochemistry Center, Heidelberg, Germany

The paralogous Brr6 and Brl1 are conserved integral membrane proteins of the nuclear envelope (NE) with an unclear role in nuclear pore complex (NPC) biogenesis. Here, we analyzed double-degron mutants of Brr6/Brl1 to understand this function. Depletion of Brr6 and Brl1 caused defects in NPC biogenesis, whereas the already assembled NPCs remained unaffected. This NPC biogenesis defect was not accompanied by a change in lipid composition. However, Brl1 interacted with Ndc1 and Nup188 by immunoprecipitation, and with transmembrane and outer and inner ring NPC components by split yellow fluorescent protein analysis, indicating a direct role in NPC biogenesis. Consistently, we found that Brr6 and Brl1 associated with a subpopulation of NPCs and emerging NPC assembly sites. Moreover, *BRL1* overexpression affected NE morphology without a change in lipid composition and completely suppressed the nuclear pore biogenesis defect of *nup116Δ* and *gle2Δ* cells. We propose that Brr6 and Brl1 transiently associate with NPC assembly sites where they promote NPC biogenesis.

Introduction

The nuclear pore complex (NPC) is a large cylindrical structure with multiple copies of more than 30 different proteins named nucleoporins (NUPs; Beck and Hurt, 2017). The NPC is embedded in the nuclear envelope (NE) at sites of inner nuclear membrane (INM) and outer nuclear membrane (ONM) fusion. The NPC promotes the bidirectional nucleocytoplasmic transport of proteins and RNA through the central channel in the NPC lumen that contains NUPs with Phe- and Gly-rich repeats (FG-NUPs; Radu et al., 1995; Strawn et al., 2004; Alber et al., 2007; Wente and Rout, 2010; Eibauer et al., 2015). Other NUPs have a structural role or embed the NPC into the NE. Some of the outer and inner ring complex components bind to the transmembrane (TM) protein Ndc1 (Gerace et al., 1982; Hallberg et al., 1993; Wozniak et al., 1994; Miao et al., 2006; Stavru et al., 2006). Interestingly, yeast Ndc1 has an additional role in inserting the spindle pole body (SPB), the functional equivalent of the human centrosome, into the NE (Winey et al., 1993; Chial et al., 1998). NE embedding of the SPB is a consequence of the closed mitosis in yeast *Saccharomyces cerevisiae*. It allows the SPB to organize nuclear and cytoplasmic microtubules, with functions in chromosome segregation and spindle positioning, respectively.

Higher eukaryotes have two pathways to assemble NPCs. One pathway assembles NPCs in telophase upon chromatin binding of the NUP ELYS/MEL28 (Loïodice et al., 2004; Gillespie et al., 2007; Hetzer and Wente, 2009; Doucet et al., 2010). In contrast, the interphase pathway promotes NPC biogenesis in the intact double membrane of the NE and is independent of ELYS/MEL28, indicating it is mechanistically distinct from the telophase NPC biogenesis (Rexach, 2009; Funakoshi et al., 2011; Vollmer et al., 2015). Recent EM data in human cells visualized membrane intermediates in interphase NPC biogenesis (Otsuka et al., 2016). Interphase NPC assembly follows, at least partially, an inside-out (nuclear to cytoplasm) extrusion of the NE that eventually leads to fusion of the double membrane. Because of the closed mitosis, *S. cerevisiae* assembles NPCs exclusively by the "interphase" pathway (Winey et al., 1997; Khmelinskii et al., 2010).

The paralogous *BRR6* and *BRL1* code for two essential integral membrane proteins of the NE in *S. cerevisiae*, with functions in NPC biogenesis or stability. Brr6, Brl1, and the nonessential Apq12, also an integral membrane protein of the NE, were found to interact with each other by immunoprecipitation (IP; Lone et al., 2015). Interestingly, deformations of the INM, so-called herniations, were observed in conditional lethal *brr6* and *brl1* cells (de Bruyn Kops and Guthrie, 2001; Hodge et al., 2010). Herniations are also a phenotype of yeast NPC mutants such as *nup116Δ* cells (Wente and Blobel, 1993). Recently, it was discovered that GLFG repeats in Nup116 stabilize critical interactions with scaffold NUPs during interphase NPC biogenesis. Failure of these interactions, as in *nup116ΔGLFG P_{MET3}-NUP188* cells, results in the formation of herniations

Check for updates

JOURNAL OF CELL BIOLOGY

(Onischenko et al., 2017). Thus, herniations can arise from faulty NPC biogenesis processes.

Conditional lethal *brr6* or *brl1* cells showed a change in lipid composition at the restrictive temperature. In addition, they grew poorly on plates with benzyl alcohol (BA), which increases membrane fluidity, and genetically interacted with mutant genes involved in lipid biogenesis (Mukhopadhyay et al., 2002; Hodge et al., 2010; Lone et al., 2015). As a result, it was suggested that Brr6 and Brl1 modulate lipid fluidity to allow NPC biogenesis. Fission yeast Brr6 (*Schizosaccharomyces pombe* lacks *BRL1*) functions in the insertion of the SPB into the NE, indicating membrane-modulating activity of this protein (Tamm et al., 2011). Whether *S. pombe* Brr6 has an additional role in NPC biogenesis has not been investigated.

Here, we analyzed the functions of Brr6 and Brl1 in *S. cerevisiae*. Because of their paralogous relationship, we constructed conditional lethal *BRR6/BRL1* double-degron mutants to analyze phenotypes. Double depletion of both proteins rapidly affected NPC biogenesis without impairing already assembled NPCs or changing lipid composition. In *BRR6/BRL1* double-degron cells, SPB duplication was only mildly affected. The SPB phenotype arose later than the NPC biogenesis defect. Brr6 and Brl1 associated with assembly intermediates of NPC biogenesis on the bend of the INM. In addition, Brl1 interacted with a range of NUPs, and *BRL1* overexpression was able to bypass the scaffolding function of Nup116 and overcome the NPC biogenesis defect of *gle2Δ* cells. We propose that Brr6 and Brl1 transiently bind to NPC assembly sites to mediate NPC biogenesis.

Results

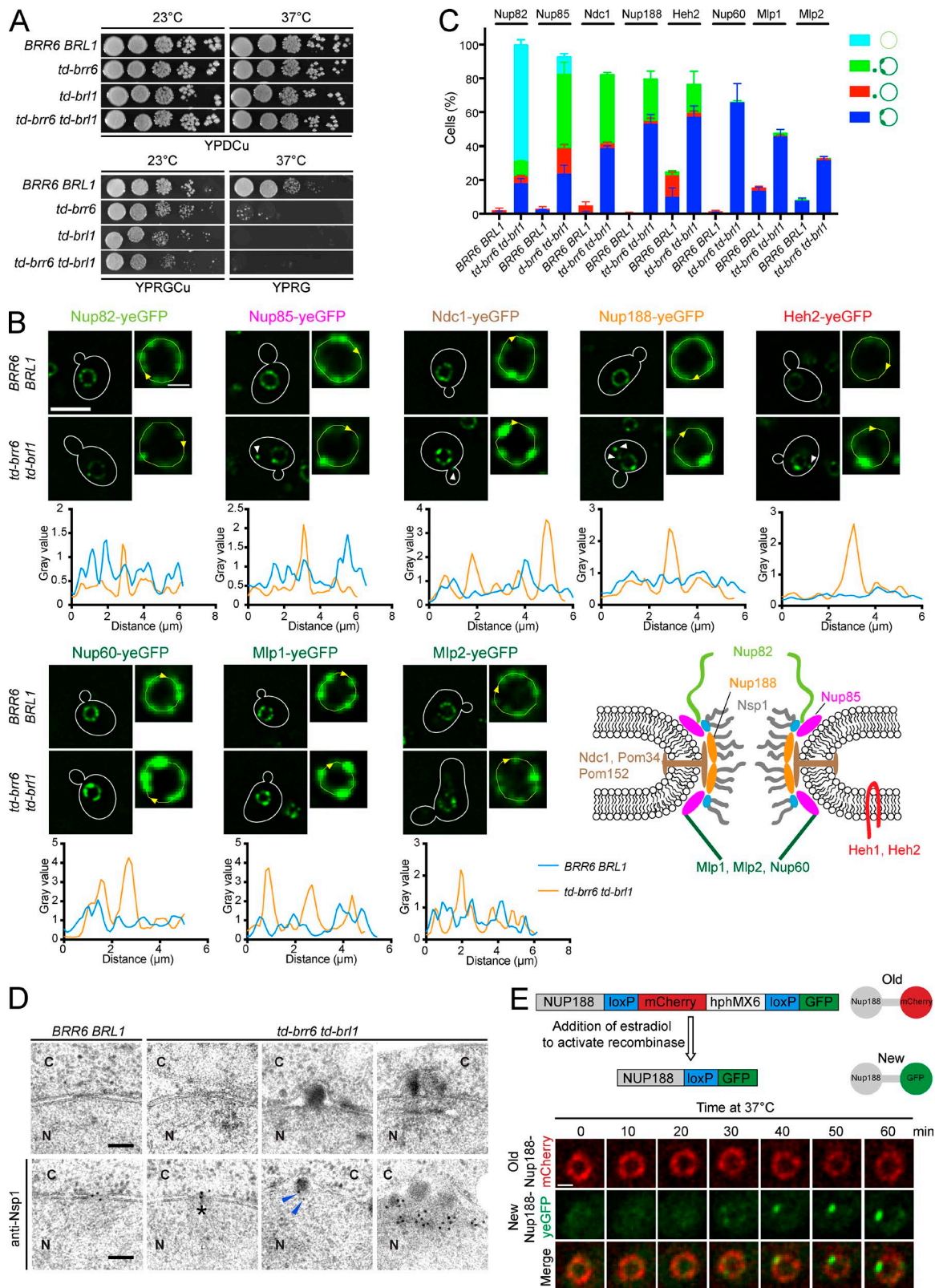### Codepletion of Brr6 and Brl1 causes NPC assembly defects

Brr6 and Brl1 are interacting paralogues that may have overlapping functions (Schneiter and Cole, 2010). To analyze the full impact of the loss of both gene products, we combined *brr6(ts)* and *brl1(ts)* alleles. However, double mutant cells showed a synthetically lethal phenotype (Fig. S1 A). We therefore combined the temperature-inducible degrons (td) *td-brr6* and *td-brl1* that were under control of the Cu^{2+}-inducible P_{CUP1} promoter. Single- or double-degron *td-brr6* and *td-brl1* cells with P_{GAL1}-*UBR1* grew at 23°C or 37°C in the presence of Cu^{2+} on yeast extract, peptone, and glucose (YPD) plates as *BRR6 BRL1 P_{GAL1}-UBR1* WT (named *BRR6 BRL1* WT) cells but were unable to grow on YPRG plates without Cu^{2+} at 37°C (Fig. 1 A). Galactose-induced expression of the E3 ligase P_{GAL1}-*UBR1* promotes degradation of the degron-tagged protein by the proteasome (Kanemaki et al., 2003). Consistently, Brr6 and Brl1 were rapidly degraded upon shifting cells to 37°C in the presence of galactose (Fig. S1 B). The temperature-dependent growth defect was complemented by the corresponding trans-genes (Fig. S1 C).

It has been reported that conditional lethal *brr6(ts)* or *brl1(ts)* mutant cells display mislocalization of cytoplasmic NUPs (Hodge et al., 2010). To evaluate whether this phenotype was also observed in the *td-brr6 td-brl1* cells and whether mislocalization was a general phenotype for all NUP subgroups, we examined the cellular localization of NUPs after 3 h at 37°C in YPRG medium (Figs. 1 B and S1 D). All NUPs showed a uniform localization along the NE in *BRR6 BRL1* WT cells. In

contrast, the majority of *td-brr6 td-brl1* cells displayed NPC defects upon degradation of Brr6 and Brl1 (Fig. 1, B and C; and Fig. S1, D and E). The signal of Nup82–yeast-enhanced GFP (Nup82-yeGFP) along the NE was reduced in *td-brr6 td-brl1* cells compared with WT control. This was also the case for Nup85, a member of the Y-shape complex. In addition, ~40% of *td-brr6 td-brl1* cells showed Nup85-yeGFP–positive dots in the cytoplasm (Fig. 1 B, arrowhead) and clustering into several dots on the NE (Fig. 1, B and C). Similar defects were observed for nearly all other NUPs, independently of their localization and function (Fig. 1, B and C; and Fig. S1, D and E). The INM protein Heh2 also showed similar mislocalization (Fig. 1, B and C). Heh2 is a member of the Lap2-emerin-MAN1 family of integral INM proteins, which binds to an early NPC assembly intermediate but not to mature NPCs (Webster et al., 2014). In contrast, we observed only minor localization defects upon Brr6/Brl1 depletion for Heh1 (Fig. S1, D and E), which functions in NPC repair (Webster et al., 2016). No defects were detectable for the ER markers Sec63-yeGFP and Ole1-yeGFP, which are not associated with NPCs (Fig. S1, F and G; Stukey et al., 1990; Delic et al., 2013). Collectively, these data show that the Brr6 and Brl1 proteins are important for proper localization of most NUPs.

We next performed EM to examine the ultrastructure of NPCs in *td-brr6 td-brl1* cells. Depletion of Brr6 and Brl1 caused NE abnormalities (Fig. 1 D). In particular, the NE showed many electron-dense inclusions beneath the INM, so-called herniations (Wente and Blobel, 1993), and sheet structures inside the nucleus. Immunostaining indicated that INM inclusions and sheets contained the FG-NUP Nsp1. The Nsp1 label was at the nuclear bottom region of the herniations (Fig. 1 D). In addition, the anti-Nsp1 antibody labeled morphologically proper NPCs in *td-brr6 td-brl1* cells (Fig. 1 D, asterisk). Thus, double depletion of Brr6 and Brl1 affects NPCs.

To evaluate whether the mislocalization of NUPs in *td-brr6 td-brl1* cells was the result of a general NPC destabilization or a defect in new NPC assembly, we compared Nup188-mCherry–marked NPCs that assembled in the presence of Brr6/Brl1 activity with Nup188-yeGFP that was synthesized after Brr6/Brl1 depletion. This experiment was done with the recombination-induced tag exchange (RITE) system (Terweij et al., 2013) that allows rapid switching of tags via Cre-induced recombination from *NUP188-mCherry* to *NUP188-yeGFP* (Figs. 1 E and S1, H–J). We inactivated Brr6/Brl1 by shifting *td-brr6 td-brl1* cells to 37°C for 1 h. This short time at 37°C was chosen to observe the impact of Brr6/Brl1 inactivation on newly assembled NPCs. With the temperature shift, Cre recombinase was activated by the addition of estradiol. The efficiency of mCherry-to-yeGFP switching during 1 h of Cre induction was ~50–60% (Fig. S1 H). In *td-brr6 td-brl1* cells, Nup188-mCherry signal, representing the assembled NPCs, remained equally distributed over the NE during the time-lapse experiment. In contrast, the newly synthesized Nup188-yeGFP accumulated as a dot on the NE (Figs. 1 E and S1 I). This phenotype was observed in ~50% of cells with Cre-induced recombination (Fig. S1 H). In the other 50% of cells, Brr6/Brl1 were probably insufficiently depleted after 1 h at 37°C to cause NPC defects. In a control experiment, we established that *BRR6 BRL1* WT cells showed equal distribution of both Nup188-mCherry and Nup188-yeGFP, when Cre recombinase was switched on (Fig. S1, H and J). These data suggest that Brr6 and Brl1 are required for the biogenesis of new NPCs but not for maintenance of already assembled NPCs.

Figure 1. **Loss of Brr6 and Brl1 cause NPC assembly defects. (A)** Serial-dilution growth assay of *td-brr6 td-brl1* cells. **(B)** Images of living cells incubated at 37°C for 3 h. The yeGFP signal along the NE was scanned (enlargement right, yellow circle) for the distribution of the NUPs (graph, bottom). Arrowheads indicate GFP-dots in the cytoplasm. A cartoon of NUPs with GFP-fusions used in B and in Fig. S1 D is shown. Bars: (overviews) 5 µm; (enlargements) 1 µm. **(C)** Percentage of cells with mislocalization of GFP-fusion proteins. Error bars: SD (*n* > 180); three independent experiments. **(D)** TEM micrographs of *BRR6 BRL1* WT and *td-brr6 td-brl1* cells incubated for 3 h at 37°C. Anti-Nsp1 staining at normal NPCs (asterisk), herniations (arrowheads), and sheets. N, nucleus; C, cytoplasm. Bars, 100 nm. **(E)** RITE assay. Estradiol induces a genetic switch of *NUP188-mCherry* (old) to *NUP188-yeGFP* (new). *td-brr6 td-brl1* cells were imaged at 10-min intervals after addition of estradiol at 37°C. Fig. S1 I shows an additional *td-brr6 td-brl1* cell. Bar, 1 µm.

Because of the SPB duplication defect of *brr6(ts)* cells in *S. pombe* (Tamm et al., 2011), we asked whether SPB duplication is also affected in *td-brr6 td-brl1* cells. Interestingly, mild SPB duplication defects were observed after 4 h at the restrictive condition (Fig. S2, A–E) when the NPC biogenesis defect was already strongly apparent (Fig. 1, B and C; and Fig. S1, D and E). In addition, yeGFP-Brl1 and yeGFP-Brr6 did not accumulate with SPBs during any cell cycle phase, including the time of the insertion of the new SPB into the NE (Fig. S2 F), as is the case in *S. pombe* (Tamm et al., 2011). Thus, because SPB defects occurred after NPC defects and because of the lack of Brr6/Brl1 enrichment at SPBs, the SPB defect in *td-brr6 td-brl1* cells may be an indirect consequence of the NPC biogenesis failure. Indeed, we have recently shown that NPCs are important for SPB duplication (Rüthnick et al., 2017).

Depletion or overexpression of Brr6 and Brl1 does not affect cellular lipid composition

Previously, it has been described that conditional lethal *brr6(ts)* cells change ergosterol and neutral lipid composition when incubated for 6 h at 37°C (Hodge et al., 2010). *brr6(ts) and brl1(ts)* cells accumulated high levels of monounsaturated and shorter-chain fatty acids after 16 h at 16°C (Lone et al., 2015). This led to the suggestion that both proteins promote NPC biogenesis by regulating lipid homeostasis. To test this model, we analyzed lipid profiles after codepletion of Brr6 and Brl1 over time and simultaneously followed the appearance of NPC defects by fluorescence microscopy. Although NPC defects were clearly detectable after 3 h at 37°C as indicated by Nup188-yeGFP clustering (Fig. 2 A), the lipid composition of *BRR6 BRL1* WT and *td-brr6 td-brl1* cells was very similar. The lipid species, the functional lipid subgroups, the chain length, and the number of double bonds were nearly identical in *BRR6 BRL1* WT and *td-brr6 td-brl1* cells (Fig. 2, B–E). Over the 6-h time course, the tendency of lipid changes was similar for both strains (Fig. 2 F). These data suggest that depletion of Brr6/Brl1 affects NPC biogenesis without changing lipid composition.

Recently, it was shown that an additional copy of *BRL1* was able to rescue cell viability of *nup116Δ* or *nup57Δ* cells (Liu et al., 2015). This rescue was attributed to a change in the lipid composition induced by elevated *BRL1*, because BA, which modulates membrane fluidity, caused decreased cell viability of *nup57Δ* cells with an extra copy of *BRL1*. In our *nup116Δ* strain background, an additional copy of *BRL1* did not allow growth of cells at 37°C (Fig. 3 A). However, expression of P_{GAL1}-*BRL1* or P_{ADH1}-*BRL1*, but not P_{GAL1}-*BRR6* or P_{ADH1}-*BRR6*, was able to suppress the growth defect of *nup116Δ* cells at 37°C (Fig. 3 A and see Fig. 7, A and B). Mass spectrometric analysis measurements did not detect changes in lipid profiles in WT cells upon P_{GAL1}-*BRR6* or P_{GAL1}-*BRL1* induction after 6 h at 30°C (Fig. 3, B–E), with the exception of a very mild increase in the chain length of certain triacylglyceride (TAG) subspecies in the case of *BRL1* overexpression (Fig. 3 D, asterisks). These data support the notion that Brr6 and Brl1 promote NPC biogenesis without affecting overall lipid composition.

Reduced growth on BA has been used as an argument for a change in lipid composition in *brr6(ts)* and *brl1(ts)* cells. To evaluate the broadness of this phenotype, we tested conditional lethal *brr6(ts)* and *brl1(ts)* mutant cells together with NPC and SPB mutants for growth on plates with BA. Fig. 3 F shows that only a subset of *BRL1* alleles (*brl1-56* at 23°C–33°C and

brl1-58 at 30°C and 33°C) grow more poorly in the presence of BA in comparison to the cells on the control plate. In contrast, BA did not enhance the growth defect of other mutant cells (*brr6-19, brr6-732,* or *brr6-751*). BA even promoted growth of *brr6-5001* cells at 33°C. No matter whether BA affected the growth or not, *brr6(ts)* and *brl1(ts)* alleles cells showed NPC defects (Fig. 3 G). Reduced growth on BA was also observed for *mps2-1, mps2-42, mps2-2, nbp1-2, nbp1-3, pom33Δ,* and *nup133Δ* cells that are defective in the insertion of the new SPB into the NE (*mps2(ts), ndc1(ts),* and *npb1(ts)*) or NPC biogenesis (*pom33Δ* and *nup133Δ*), but do not have a direct impact on lipid biosynthesis.

Partial NPC localization of Brr6 and Brl1

To better understand the function of Brr6 and Brl1 in NPC biogenesis, we analyzed the localization and topology of both proteins. Brr6 and Brl1 have been reported to localize to the NE and ER using plasmid-encoded tagged versions of the genes that were expressed in parallel to the untagged WT gene copy (de Bruyn Kops and Guthrie, 2001; Saitoh et al., 2005). To confirm this localization, we fused *BRR6* and *BRL1* to yeGFP and moderately overexpressed the gene fusions from the P_{ADH1} promoter (Fig. 4 A). Brr6 and Brl1 localized at both the NE and the peripheral ER independently of the position of the yeGFP tag (Fig. 4 A). The intensity of yeGFP-Brr6 and Brr6-yeGFP at the cell cortex was stronger than that at the NE. This ratio was reversed for yeGFP-Brl1 and Brl1-yeGFP (Fig. 4 A). The uniform NE localization of yeGFP-Brl1 and yeGFP-Brr6 was disturbed in *apq12Δ* cells grown at the restrictive temperature. Both proteins showed a punctate pattern in *apq12Δ* cells (Fig. S3 A, arrowheads). Thus, Brr6 and Brl1 are uniformly distributed along the NE, in dependence on Apq12.

Tagging of *BRR6* and *BRL1* at the 3′ end by yeGFP without affecting the promoter confirmed localization of both proteins at the nuclear rim that was marked by Nup188-tdTomato (Fig. 4 B). Scanning of the fluorescence intensities along the NE indicated a fraction of overlapping peak intensities between Brr6/Brl1 and Nup188 (Fig. 4 B, arrowheads). This may indicate localization of Brr6/Brl1 to a subpopulation of NPCs. To test this further, we performed immuno-EM using anti-GFP antibodies followed by protein A–gold (Fig. 4, C–E). The membrane NUP yeGFP-Pom34 was used as control for a NE-associated protein that localizes with NPCs. Asi3-yeGFP, a protein of the INM with a function in quality control (Khmelinskii et al., 2014), is at the NE but not at NPCs. Incubation of the yeGFP-tagged cells with only protein A–gold did not result in a NE or NPC signal. In P_{ADH1}-*yeGFP-POM34* cells, gold particles reflecting the localization of yeGFP-Pom34 were at the NE and NPCs. For yeGFP-Pom34, ~40% of the gold particles at the NE associated with NPCs (Fig. 4, C and D). In contrast, only 10% of the Asi3-yeGFP signal along the NE overlapped with NPCs. The Asi3-yeGFP signal at NPCs was similar to the NPC occupancy of the NE (Fig. 4 D) and therefore probably reflects Asi3 molecules that were coincidently close to NPCs at the time of fixation. Interestingly, 20–25% of the NE-associated Brr6 and Brl1 signals were at NPCs. This number was lower than that for Pom34 but clearly higher than the 10% value for Asi3. We therefore conclude that a fraction of Brr6 and Brl1 associates with NPCs.

We next used the immuno-EM data from Fig. 4 C to quantify the INM and ONM distribution of Brr6 and Brl1. The Asi3 signal was predominantly associated with the INM, consistent
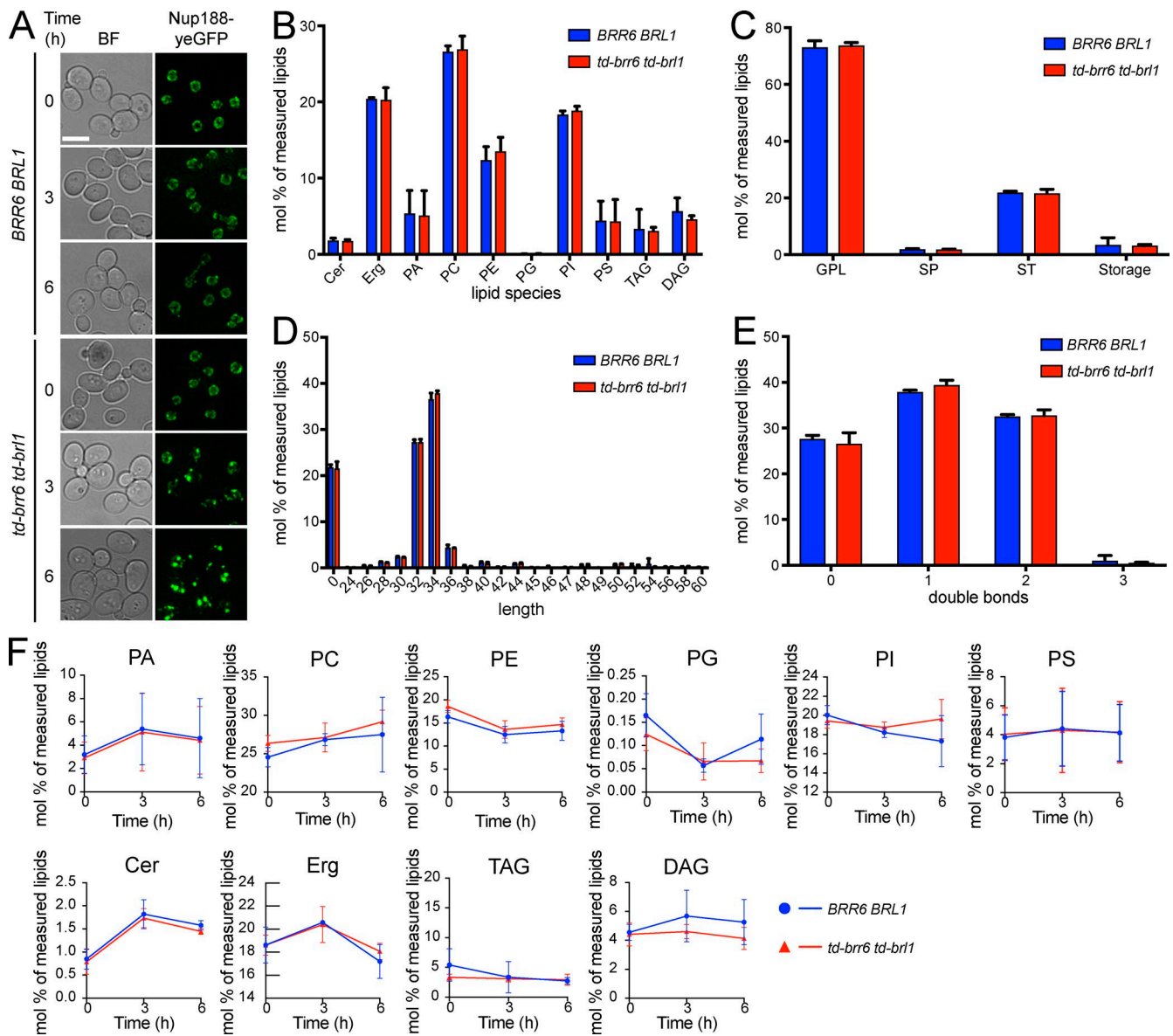
Figure 2. **Codepletion of Brr6 and Brl1 does not affect lipid composition. (A)** Cells were incubated at 37°C as in Fig. 1 B and analyzed 0, 3, and 6 h after temperature shift with Nup188-yeGFP as NPC marker. Images with maximum-intensity projections are shown. Bar, 5 µm. **(B–F)** Lipids were extracted from cell cultures used for A with subsequent mass spectrometric analysis by nano-ESI-MS/MS. Samples in B–E were analyzed after 3 h at 37°C. (B) Lipid classes displayed as mol% of measured lipids. (C) Distribution of lipids into functional categories of glycerophospholipids and glycerolipids (GPL), sphingolipids (SP), sterols (ST), and storage lipids. (D) Chain length profiles. (E) Double bond profiles. (F) Changes in the mol% distributions of lipid classes during the time course experiment. Error bars in B–F: SD (n = 3).

with published data (Zargari et al., 2007; Fig. 4, C and E). yeGFP-Brr6 and Brr6-yeGFP were equally distributed on both sides of the NE, whereas yeGFP-Brl1 mainly localized to the INM (Fig. 4, C and E). Thus, Brr6 and Brl1 associate with the INM; Brr6 shows additional localization at the ONM.

Membrane topology of Brr6 and Brl1

Brr6 and Brl1 are integral membrane proteins, although their topology is a matter of debate (de Bruyn Kops and Guthrie, 2001; Kim et al., 2006). To elucidate the topology of Brr6 and Brl1, we used the bifunctional complementation (BiFC) assay (Hu et al., 2002). In this assay, C- and N-terminal domains of Venus (VC and VN) that are nonfluorescent are expressed as gene fusions. As soon as VC and VN come close together, because either two fusion proteins interact or N and

C termini of an integral membrane protein are on the same side of the membrane, VC and VN interact and the YFP is restored. Following this strategy, *VN-BRL1-VC* fusions were expressed as the only chromosomal copy. The VN-Brl1-VC signal was detectable at the NE (Fig. 4 F). In contrast, the integral membrane protein VN-Pom152-VC, which only has one membrane-spanning domain (Tcheperegine et al., 1999), did not show a YFP signal (Fig. 4 F). This indicates that N and C termini of Brl1 are located on the same side of the NE. In contrast to *VN-BRL1-VC* cells, tagging of BRR6 on both sides (*VN-BRR6-VC*) strongly affected viability of cells. We therefore combined *VC-BRR6* with *BRL1-VN* and *BRR6-VN* with *VC-BRL1* (Fig. S3 B). Both combinations resulted in YFP-positive cells, suggesting that N and C termini of Brr6 are adjacent to the N and C termini of Brl1.
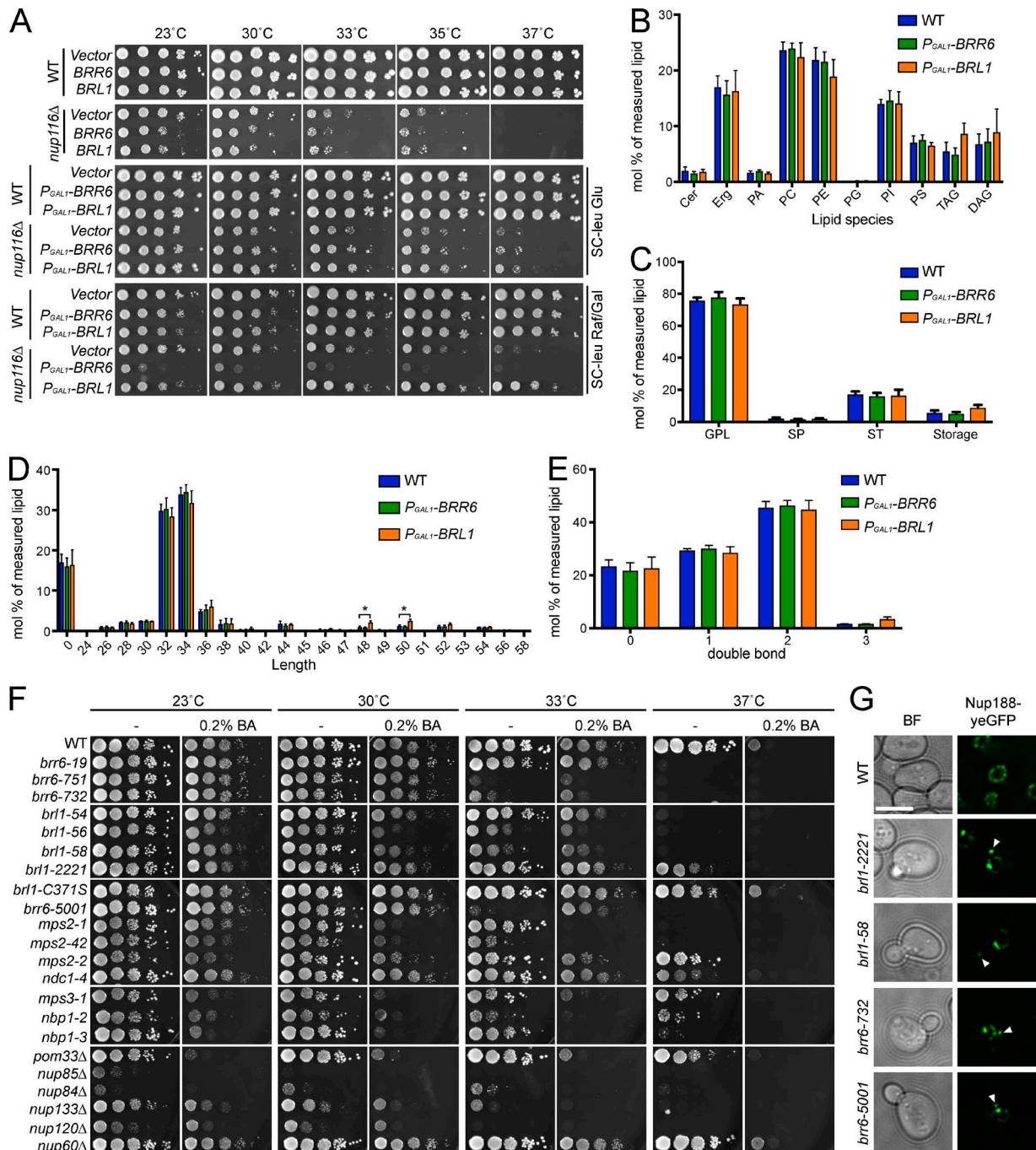
Figure 3. **Overexpression of *BRR6* or *BRL1* does not cause lipid alterations, but *BRL1* overexpression rescues growth of *nup116Δ* cells.** **(A)** Growth of WT and *nup116Δ* cells with the indicated plasmids. **(B–E)** Lipid composition analysis of WT, P_{GAL1}-*BRR6* and P_{GAL1}-*BRL1* cells (6-h induction at 30°C) by nano-ESI-MS/MS. The description is the same as in Fig. 2 (B–E). Error bars in B–E: SD (*n* = 3). Unpaired *t* test with two-tailed *p*-value was used to compare the samples in D; *, P ≤ 0.05. **(F)** Growth of yeast cells on BA plates. **(G)** NPC phenotype of WT and *brr6(ts)* and *brl1(ts)* cells incubated for 3 h at 37°C. Arrowheads indicate GFP-dots in the cytoplasm. Bar, 5 µm.

Previous data suggest that the C termini of Brr6 and Brl1 are exposed to either the cytoplasm or nucleoplasm (Smoyer et al., 2016). Confirmation of this conclusion came from histidine-biotin-histidine (HBH)–tagged Brr6. The HBH tag of HBH-Brl1, HBH-Brr6, and Brr6-HBH became biotinylated, as indicated by streptavidin detection (Fig. 4 G). Because the biotin modification system is not localized in the nuclear intermembrane space (Huh et al., 2003; Emerman et al., 2010), this result confirms that the N and C termini of

Brr6 and the N terminus of Brl1 are localized in either the nucleoplasm or cytoplasm.

Disulfide bonds are important for localization and stability of Brl1

Four conserved cysteine residues are found in all Brr6/Brl1 orthologues (Fig. 4 H). Importantly, Brl1 contains two additional cysteine residues in its second TM domain (Fig. 4 H; TM2). Because the nuclear intermembrane space has an oxidative
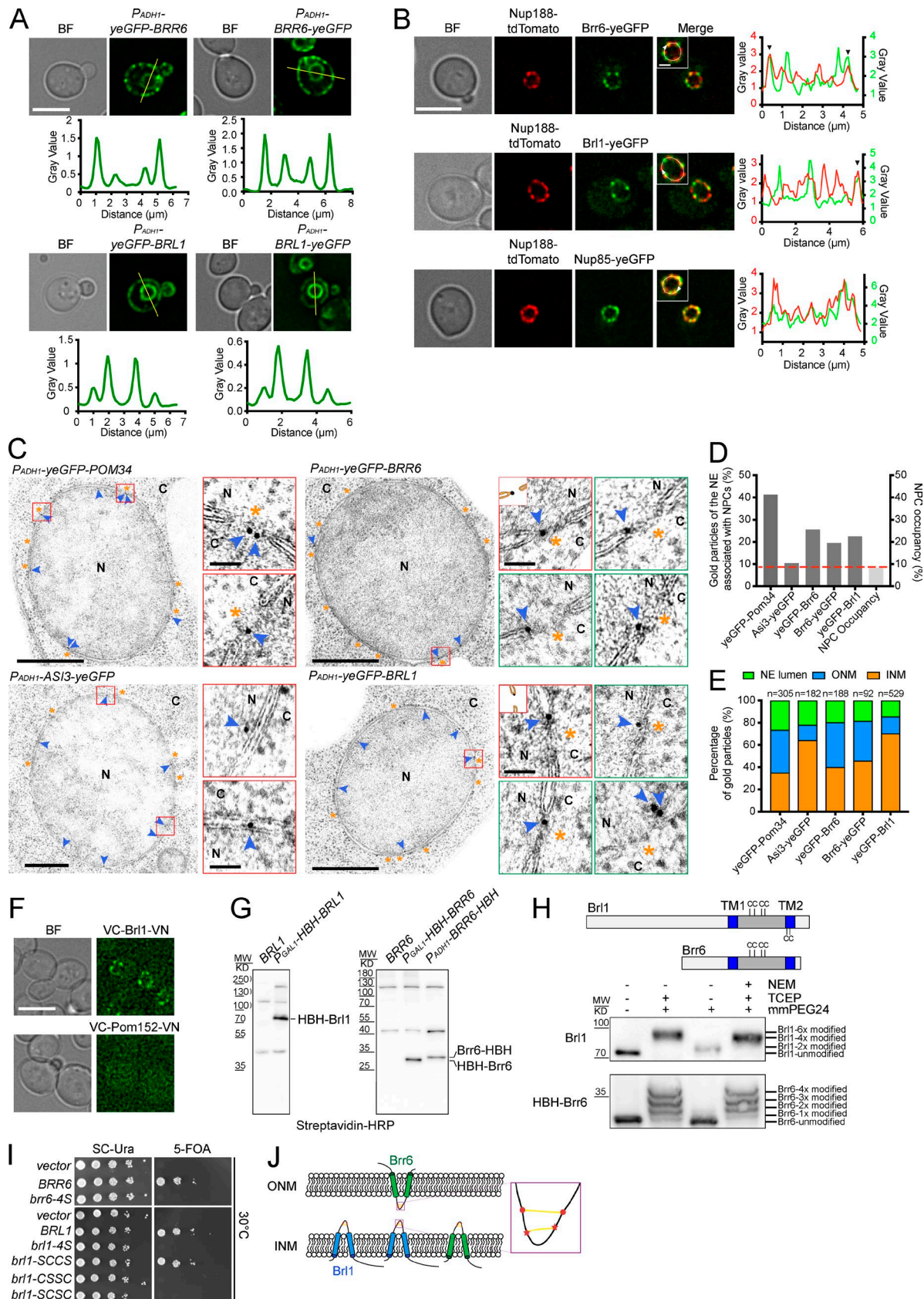
Figure 4. **Brr6 and Brl1 localization and the role of disulfide bonds. (A)** Localization of yeGFP-tagged Brr6 and Brl1 expressed under control of P_{ADH1}. Plot profiles along the yellow lines indicate the distribution of yeGFP signals on the NE and the cortical ER. Bar, 5 µm. **(B)** Strains expressing *NUP188-td-Tomato* in combination with *BRR6-yeGFP*, *BRL1-yeGFP*, or *NUP85-yeGFP* under the endogenous promoter. The enlargements (top left) show NEs that were used for the plot profiles (right). Black arrowheads in the graph indicate colocalization of Brr6 or Brl1 with Nup188 on the NE. Bars: (overview) 5 µm;

environment (Braakman et al., 1991; Frand et al., 2000), we determined the redox state of the cysteine residues in Brr6 and Brl1 to judge whether they localize in the intermembrane space or in the nucleus/cytoplasm.

Analysis of yeGFP-Brr6 and Brl1 by SDS-PAGE under oxidative and reducing conditions excluded the possibility of intermolecular interactions via disulfide bridges (Fig. S3 C), as we failed to detect dimeric or multimeric GFP-Brr6 or Brl1 species in the absence of the reducing agent DTT. Incubation of protein extracts with 24-methyl-polyethylenglycol-maleinimide (mmPEG24), which alkylates free cysteine residues and causes an upshift of the protein in SDS-PAGE upon modification, did not affect running behavior of the HBH-tagged version of Brr6 (HBH tag does not contain cysteine; Fig. 4 H, lane 1 and 3). mmPEG24 triggered only a small upshift of Brl1 (Fig. 4 H, lanes 1 and 3). This indicates that most cysteine residues in both proteins were oxidized. To confirm this notion, we preincubated the cell extract with Tris-2-carboxyethyl-phosphine (TCEP) to reduce all cysteine residues followed by mmPEG24 incubation. This scheme resulted in four mmPEG24-modified HBH-Brr6 bands. Brl1 was strongly upshifted into one band (Fig. 4 H, lane 2). This result further indicates that cysteine residues in Brr6 and Brl1 are predominately oxidized in vivo.

To exclude that cysteine residues became oxidized during extract preparation, intact cells were first incubated with the membrane-permeable *N*-ethylmaleimide (NEM) to block all free cysteines. Cell extracts were then treated with TCEP and mmPEG24. HBH-Brr6 behaved as without NEM incubation (Fig. 4 H, compare lanes 2 and 4), indicating that all cysteine residues of Brr6 are oxidized in cells. The mmPEG24-induced upshift of Brl1 was slightly reduced by NEM (Fig. 4 H, compare lanes 4 and 2). The two cysteine residues in the TM2 domain of Brl1 are probably in a reduced state, and their blockage by NEM slightly reduced the mmPEG24-induced mobility shift.

To test for the importance of the disulfide bonds, we mutated cysteine residues in Brr6 and Brl1 to serine (C-S). Mutating all four central cysteine residues of Brr6 and Brl1 caused cell death (Fig. 4 I, *brr6-4S* and *brl1-4S*). Interestingly, *brl1-SCCS* supported viability of *brl1Δ* cells, whereas *brl1-CSSC* or *brl1-SCSC* cells failed to form colonies (Fig. 4 I). This suggests that the critical disulfide bond is the most inner one. Indeed, the full upshift of Brl1-SCCS by mmPEG24 was seen only after TCEP reduction, suggesting that the two inner cysteines of Brl1 form a disulfide bond (Fig. S3, D and E).

Why are the cysteine mutants of Brl1 nonfunctional? Analysis of cell extracts by immunoblotting indicated that P_{ADH1}-*yeGFP-brl1-SCCS* was expressed similarly to P_{ADH1}-*yeGFP-BRL1* (Fig. S3 H). yeGFP-Brl1-SCCS still localized to the NE; however, the intensity of this signal was reduced compared with WT Brl1 (Fig. S3, F and G). This reduction in signal intensity by similar expression to WT Brl1 is explained by mislocalization or misfolding of a portion of the yeGFP-Brl1-SCCS protein. P_{ADH1}-*yeGFP-brl1-4S* and P_{ADH1}-*yeGFP-brl1-*

SCSC were less expressed than P_{ADH1}-*yeGFP-BRL1* (Fig. S3 H). Consistently, the NE signal of yeGFP-brl1-4S and yeGFP-brl1-SCSC was reduced (Fig. S3, F and G). *yeGFP-brl1-CSSC* was degraded to the level of yeGFP that uniformly stained the cytoplasm. These data indicate that, at least for the overexpressed proteins, the disulfide bonds in Brl1 are important for either protein stability (inner C-C) or proper NE localization (outer C-C). A model for disulfide bond formation in Brr6 and Brl1 is given in Fig. 4 J.

Brl1 interacts with a subset of NUPs

Because Brr6 and Brl1 are not stable components of NPCs, both proteins may only transiently interact with NPCs during biogenesis. We tested the possibility of transient Brl1-NUP interactions using the BiFC assay (Hu et al., 2002). In this assay, transient interactions are preserved after YFP formation (Kerppola, 2008; Khmelinskii et al., 2014). We observed interaction of Brl1 with structural NUPs, including the TM NUPs Ndc1 and Pom33; the outer ring NUPs Nup84, Nup85, and Nup133; and the inner ring NUPs Nup188 and Nup59. Brl1 mildly interacted with Heh1 but not Heh2, which has been indicated to be involved in the quality control of NPC biogenesis (Webster et al., 2016). In contrast, no interaction was observed between Brl1 and the FG-repeat proteins Nup49 and Nup116, the cytoplasmic filament protein Nup82, and nuclear basket NUPs Nup2, Nup60, Mlp1, and Mlp2 (Fig. 5, A and B). Deletion of *APQ12* increased Nup84-Brl1 interaction in the BiFC assay but had no impact on other interactions (Fig. S3 I).

To confirm interactions, Brr6-3yeGFP and Brl1-3yeGFP were immunoprecipitated from whole-cell extracts with GFP-Trap beads (Rothbauer et al., 2008). As positive control for IP, we confirmed complex formation between Brl1 and Brr6 (Fig. S3 J; Lone et al., 2015). We detected Ndc1-6HA in the IP of Brr6-3yeGFP (Fig. 5 C). In a similar way, we detected Nup188-6HA and Ndc1-6HA bound to yeGFP-Brr6 and yeGFP-Brl1 (Fig. 5 D). Collectively, these data show that Ndc1 and Nup188 are in relatively stable complexes with Brr6 and Brl1.

Clustered Brr6 and Brl1 proteins recruit NUPs to the NE

To obtain additional evidence for the interaction of Brr6 and Brl1 with NUPs, we asked whether clustering of Brr6 and Brl1 in the NE had the ability to recruit NPCs. We induced Brr6/Brl1 clustering by galactose-induced expression of three tandem copies of the gene coding for the GFP-binding protein (3GBP; Rothbauer et al., 2008) in *BRR6-3yeGFP BRL1-3yeGFP* cells (Fig. 6 A). This expression reduced growth of *BRR6-3yeGFP BRL1-3yeGFP* cells but not of *BRR6 BRL1* cells (Fig. 6 B). Short P_{GAL1}-*3GBP* expression clustered Brr6/Brl1-3yeGFP into a dot-like region at the NE that was stronger in intensity than the Brr6/Brl1-3yeGFP signal along the NE (Fig. 6 C, arrowheads). Importantly, Nup188-mCherry was recruited to this Brr6/Brl1-3yeGFP dot, as indicated by the colocalization of yeGFP and

(enlargement) 1 µm. **(C)** Immuno-EM analysis of yeGFP-Pom34, Asi3-yeGFP, yeGFP-Brr6, and yeGFP-Brl1 cells with anti-GFP antibody. Blue arrowheads, 10-nm gold particles reflecting yeGFP localization. Orange stars indicate NPCs. Red squares represent the red marked enlargements on the right. Green boxed pictures on the right show additional examples with Brr6 and Brl1 signals at NPCs taken from other EM micrographs. N, nucleus; C, cytoplasm. Bars: (overviews) 500 nm; (enlargements) 50 nm. **(D)** Plot of gold particles of the NE at NPCs. *n* is given in E. NPC occupancy is described in Materials and methods. **(E)** Quantification of gold-labeled particles on different sides of the NE. **(F)** Topology of Brl1 by BiFC. Bar, 5 µm. **(G)** In vivo biotinylation of HBH-Brl1, HBH-Brr6, and Brr6-HBH. **(H)** Scheme of Brl1 and Brr6. In vivo redox analysis of Brr6 and Brl1. Immunoblot with antibodies against Brl1 or His-tag. **(I)** Serial dilutions of *brl1Δ CEN-URA3-BRL1* cells with the indicated *LEU2*-based CEN plasmids. 5-FOA removes the *URA3*-based plasmid. **(J)** Model for the topology of the disulfide bonds in Brr6 and Brl1.
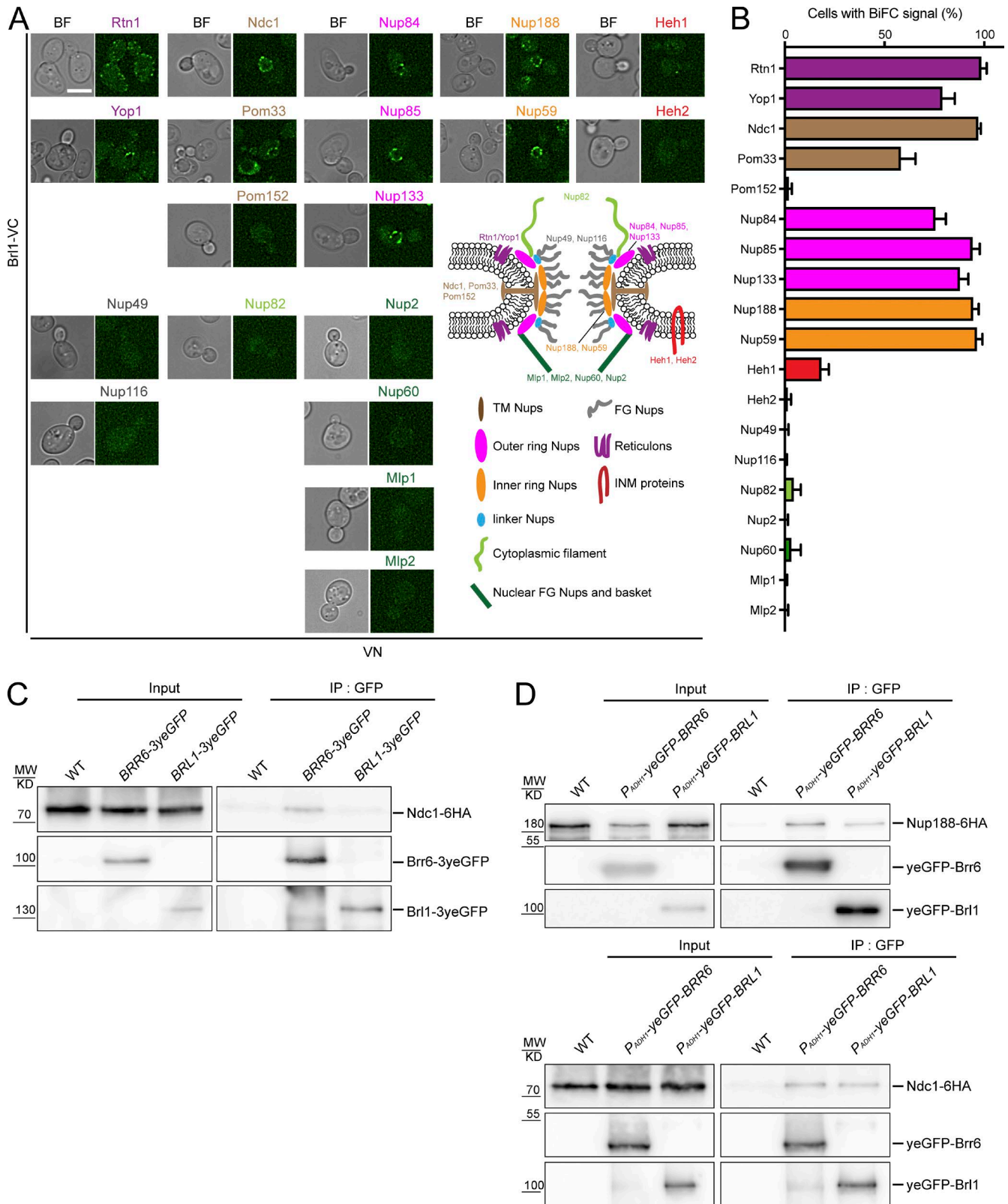
Figure 5. **Brr6 and Brl1 interact with structural NUPs that are required for the early NPC assembly. (A)** BiFC fluorescent signals of cells expressing Brl1-VC and NUP-VN fusions. A cartoon of the NPC with indicated VN-fusions is shown. Bar, 5 μm. **(B)** Quantification of cells from A. Error bars: SD (*n* > 100); three independent experiments. **(C)** Ndc1-6HA coimmunoprecipitates with Brr6-3yeGFP. **(D)** Nup188-6HA and Ndc1-6HA copurifies with yeGFP-Brr6 and yeGFP-Brl1.

mCherry (Fig. 6, C [right] and D). Expression of *P_{GAL1}-3GBP* in *NUP188-mCherry* cells had no impact on the localization of Nup188-mCherry, excluding binding of the mCherry moiety to 3GBP (Fig. S3, K and L). As a specificity control, we established that expression of *P_{GAL1}-3GBP* in *SEC63-3yeGFP* or *OLE1-3yeGFP* cells clustered Sec63-3yeGFP and Ole1-3yeGFP without affecting Nup188-mCherry localization (Fig. 6, E and F; and Fig. S3, M and N). Together with the BiFC, immuno-EM, and IP data, this supports the notion that Brr6 and Brl1 can interact with NUPs at the NE.

BRL1 overexpression suppresses the NPC biogenesis defect of *nup116Δ* and *gle2Δ* cells

Cells with a deletion of *NUP116* or *GLE2* or carrying the conditional lethal *gle2-1* allele have a growth defect at 37°C that was suppressed by *BRL1* but not *BRR6* expressed from the *GAL1* or *ADH1* promoter (Fig. 7, A and B). *GLE2* encodes for a NPC component that interacts with Nup116 (Murphy et al., 1996; Suntharalingam and Wente, 2003; Lutzmann et al., 2005). Suppression of the growth defect of *nup116Δ* cells by Brl1 was dependent on the presence of the inner cysteine residues (Fig. 7 B). Recently, it was shown that the GLFG repeats of Nup116 function in a redundant manner with Nup188 in NPC biogenesis (Onischenko et al., 2017). As for *nup116Δ* cells, the growth defect of *nup116ΔGLFG P_{MET3}-NUP188* cells was suppressed by *P_{ADH1}-BRL1* but not by *P_{ADH1}-BRR6* (Fig. 7 C). In contrast, *P_{GAL1}-BRL1* did not allow growth of *nup120Δ* and *sec13-34* cells, which also form herniations at the restrictive temperature (Fig. 7 A). *NUP120* and *SEC13* code for components of the Y-shape Nup84 complex that forms an NPC scaffold (Siniossoglou et al., 2000). In the reverse experiment, we asked whether *P_{ADH1}-NUP116* was able to suppress *brr6(ts)* and *brl1(ts)* mutant alleles. *P_{ADH1}-NUP116* allowed growth of *nup116Δ* cells at 37°C (Fig. 7 D). However, *P_{ADH1}-NUP116* did not suppress the growth defect of *brr6(ts)* or *brl1(ts)* cells (Fig. 7 D). This genetic analysis suggests that *BRL1* overexpression bypasses the functions of *NUP116* and *GLE2* in NPC biogenesis.

To understand the suppression of the *nup116Δ* and *gle2Δ* phenotypes by *P_{ADH1}-yeGFP-BRL1,* we analyzed these cells by EM. The herniation phenotype of *nup116Δ* and *gle2Δ* cells at 37°C (Fig. 7 E; Wente and Blobel, 1993; Murphy et al., 1996) was completely suppressed by *P_{ADH1}-yeGFP-BRL1* (Fig. 7 F). As in WT cells (Fig. 4, C and E), yeGFP-Brl1 localized with the smooth INM in *nup116Δ* and *gle2Δ* cells, as determined by immuno-EM (Fig. 7 F, arrowheads). Thus, Brl1 can efficiently overcome the NPC biogenesis defect of *nup116Δ* and *gle2Δ* cells.

Brr6 and Brl1 locate to NPC assembly intermediates

To understand where Brr6 and Brl1 function during NPC biogenesis, we determined their localization during the NPC assembly. NPC assembly intermediates are transient in nature and have not been described in WT yeast cells. We accumulated such structures using conditional lethal *td-brr6* or *td-brl1* cells. In light microscopy images, ~30% of *td-brr6* cells with *P_{ADH1}-yeGFP-BRL1* (Fig. 8 A) showed dot-like Nup85-tdTomato signals at the NE, most of which colocalized yeGFP-Brl1 puncta (Fig. 8, B and C). This raises the possibility that Brl1 associates with NPC assembly intermediates.

Analysis of *td-brr6* cells by EM identified INM evaginations that were labeled by the marker Nsp1 (Fig. 8 D). We

subgrouped Nsp1-labeled evaginations into three classes according to their depth (Fig. 8 F). With depth less than 30 nm, which was smaller than the INM–ONM distance (Fig. 8 F, right), we defined the INM deformations as NPC assembly intermediates. These small INM evaginations were detected in only one serial section and are therefore not extensions of herniations. The morphology of these structures was similar to NPC assembly intermediates of human cells (Otsuka et al., 2016). NE deformations, which were deeper than the ONM–INM distance, were named small or large herniations, depending on the depth of the deformation (Fig. 8 F). The diameter of herniations was similar to that of NPCs (Fig. 8 G). yeGFP-Brl1 was detected at the bend of the INM of assembly intermediates (Figs. 8 D and S4 A). The yeGFP-Brl1 signal localized mostly at the bend of the INM in small and large herniations (Fig. 8 D, middle and right).

In *td-brl1* cells, yeGFP-Brr6 was also detected at NE evaginations (Fig. 8 E). Consistent with the localization of Brr6 to the INM and ONM in WT cells (Fig. 4, C and E), Brr6 localized on both membranes of NE evaginations (Fig. 8 E). Because *BRR6* did not suppress the defect of *nup116Δ* and *gle2Δ* cells (Figs. 3 A and 7 A), we could use these cells for analysis of the localization of yeGFP-Brr6. yeGFP-Brr6 localized to the INM and ONM of herniations (Fig. S4, B and C). In summary, Brl1 associates with the INM of NPC biogenesis intermediates, whereas Brr6 was at the INM and ONM of these assemblies.

To test whether Brl1 has membrane-remodeling activity, we overexpressed *BRL1* from the galactose promoter (*P_{GAL1}-BRL1*) and analyzed NE morphology. Indeed, galactose-induced expression of *P_{GAL1}-BRL1* affected the morphology of the NE in WT cells (Fig. S4, D–F). In 83% of the *P_{GAL1}-BRL1* cells (10 of 12 cells), sheets of NE were detected inside the nucleus by EM (Fig. S4 G). Such defective NE structures were not observed in control cells. This phenotype was not observed for *P_{GAL1}-BRR6* cells. Thus, Brl1 has the potential to remodel the NE.

Discussion

Brr6 and Brl1 are two integral membrane proteins of the NE with functions in NPC biogenesis (Schneiter and Cole, 2010). It was suggested that both proteins regulate lipid homeostasis, explaining their essential role in NPC biogenesis. Although this model is appealing, indications are missing for how Brr6 and Brl1 would regulate lipid composition and whether NPC defects and lipid changes correlate over time in conditional lethal *brr6(ts)* and *brl1(ts)* cells.

Because Brr6 and Brl1 are paralogues with overlapping functions, as suggested by similar NPC defects and the synthetically lethal phenotype of mutant alleles, we codepleted Brr6 and Brl1 to see the full range of Brr6 and Brl1 functions. These double-degron cells showed NPC biogenesis defects, as has been reported for the conditional lethal *brr6(ts)* and *brl1(ts)* cells (de Bruyn Kops and Guthrie, 2001; Saitoh et al., 2005; Hodge et al., 2010; Lone et al., 2015). However, lipid mass spectrometry analysis did not indicate a change in lipid composition in response to Brr6 and Brl1 depletion. In addition, *P_{GAL1}-BRR6* and *P_{GAL1}-BRL1* overexpression did not affect lipid composition. The only exception was a very small increase of TAG subspecies with long fatty acids by *P_{GAL1}-BRL1* expression. However, it is unlikely that this minute increase has an impact on the NE, because TAGs are mainly components of lipid droplets, which do not have a direct role in membrane curvature
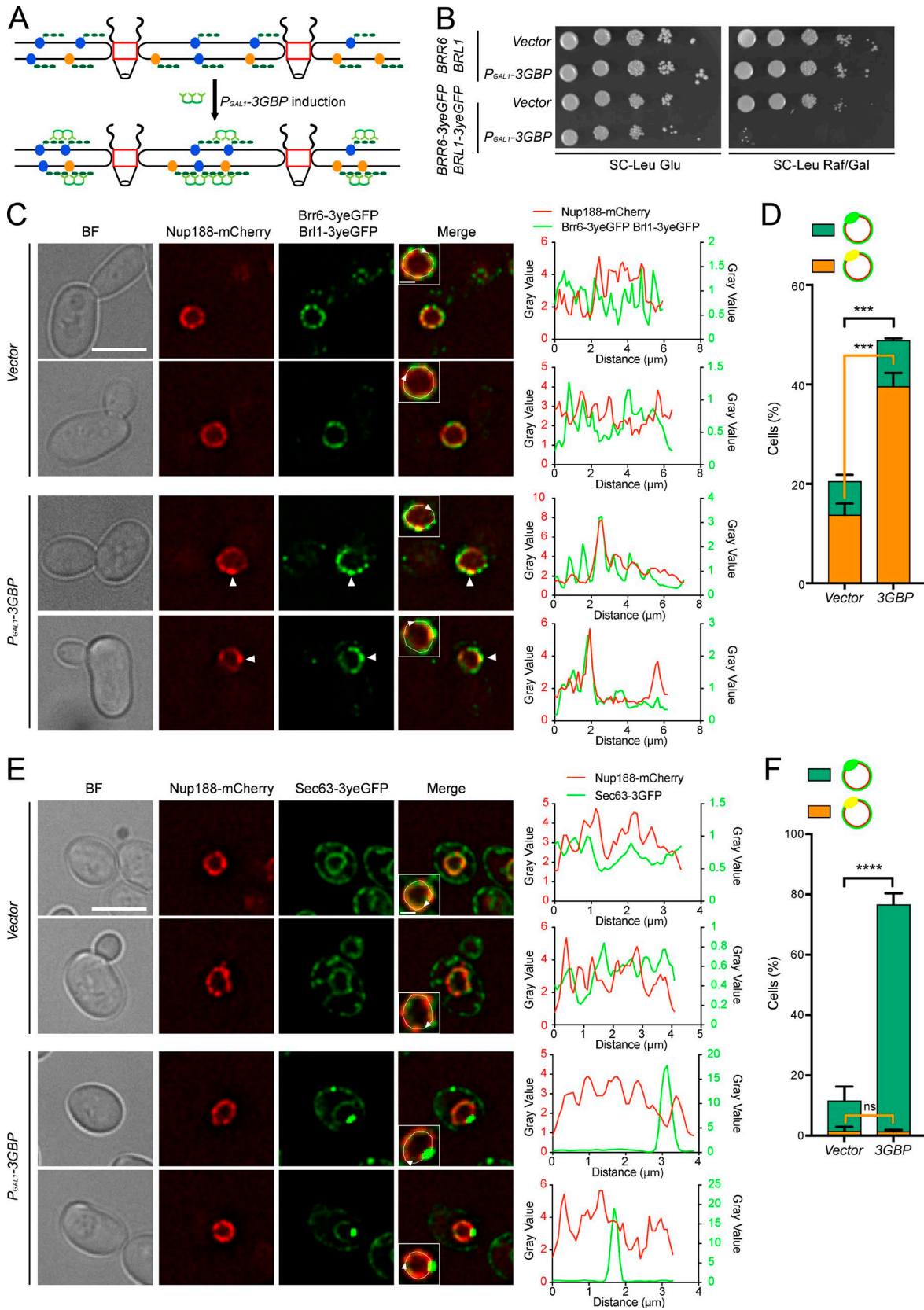
Figure 6. **In vivo cross-linking of Brr6 and Brl1 recruits Nup188. (A)** Principle of 3GBP in vivo cross-linking assay. **(B)** Growth of indicated cells with plasmids p415Gal or p415Gal-*3GBP*. **(C and E)** p415Gal or p415Gal-*3GBP* cells were incubated for 3 h at 30°C with galactose to induce the P_{GAL1} promoter. The enlargements show NEs that were used for the plot profiles on the right. Arrowheads indicate colocalization of Brr6/Brl1 and Nup188. Bars: (overviews) 5 µm; (enlargements) 1 µm. **(D and F)** Quantification of cells from C and E. Error bars: SD ($n > 300$ for C and $n > 150$ for E); three independent experiments. Unpaired *t* test with two-tailed *p*-value was used to compare the samples. ***, P ≤ 0.001; ****, P ≤ 0.0001; ns, not significant.
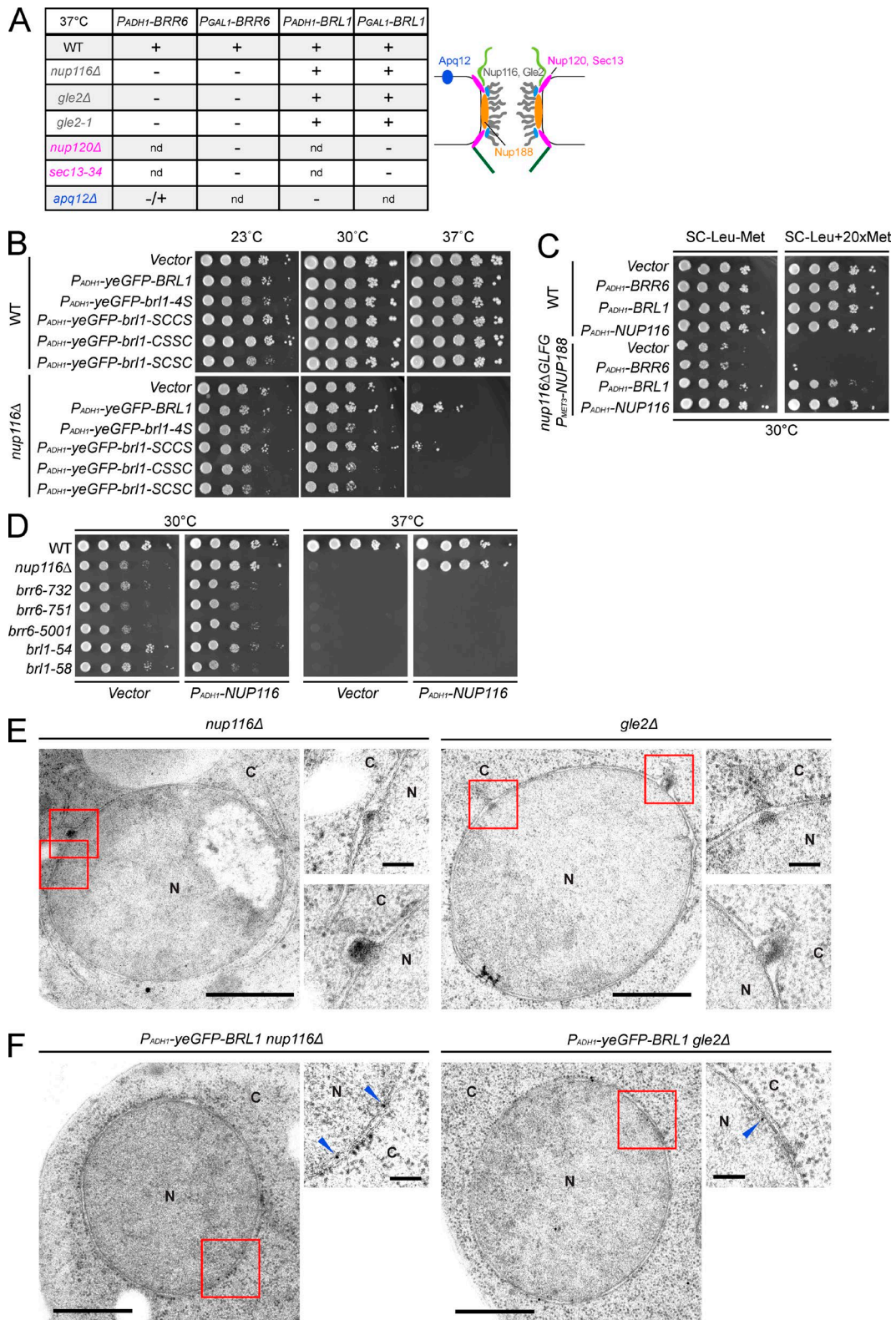
Figure 7. **Genetic interactions of *BRL1*. (A)** Indicated yeast strains with chromosomal P_{ADH1}-*BBR6* or P_{ADH1}-*BRL1* or plasmid encoded P_{GAL1}-*BRR6* or P_{GAL1}-*BRL1* were incubated for 2 d at 37°C. –, no growth; +, growth; –/+, partial growth; nd, not determined. A cartoon of the NPC with indicated proteins tested in the assay is shown. **(B)** Serial dilutions of indicated strains with the plasmid-encoded *BRL1* alleles on SC-selection plates. **(C)** Suppression of the growth defect of *nup116ΔGLFG P_{MET3}-NUP188* cells by P_{ADH1}-*BRL1*. Ten-fold serial dilutions of cells on plates with or without methionine. **(D)** Growth of *brr6(ts), brl1(ts),* and *nup116Δ* cells with P_{ADH1}-*NUP116*. **(E)** TEM images of *nup116Δ* and *gle2Δ* cells show herniation defects after incubation at 37°C for 3 and 2.5 h, respectively. N, nucleus; C, cytoplasm. Bars: (overviews) 500 nm; (enlargements) 100 nm. **(F)** Immuno-EM analysis with anti-GFP antibody. *nup116Δ* and *gle2Δ* cells with P_{ADH1}-*yeGFP-BRL1* were incubated for 3 and 2.5 h at 37°C, respectively. Arrowheads, 10-nm gold particles reflecting yeGFP localization. Abbreviations and bars are as in E.
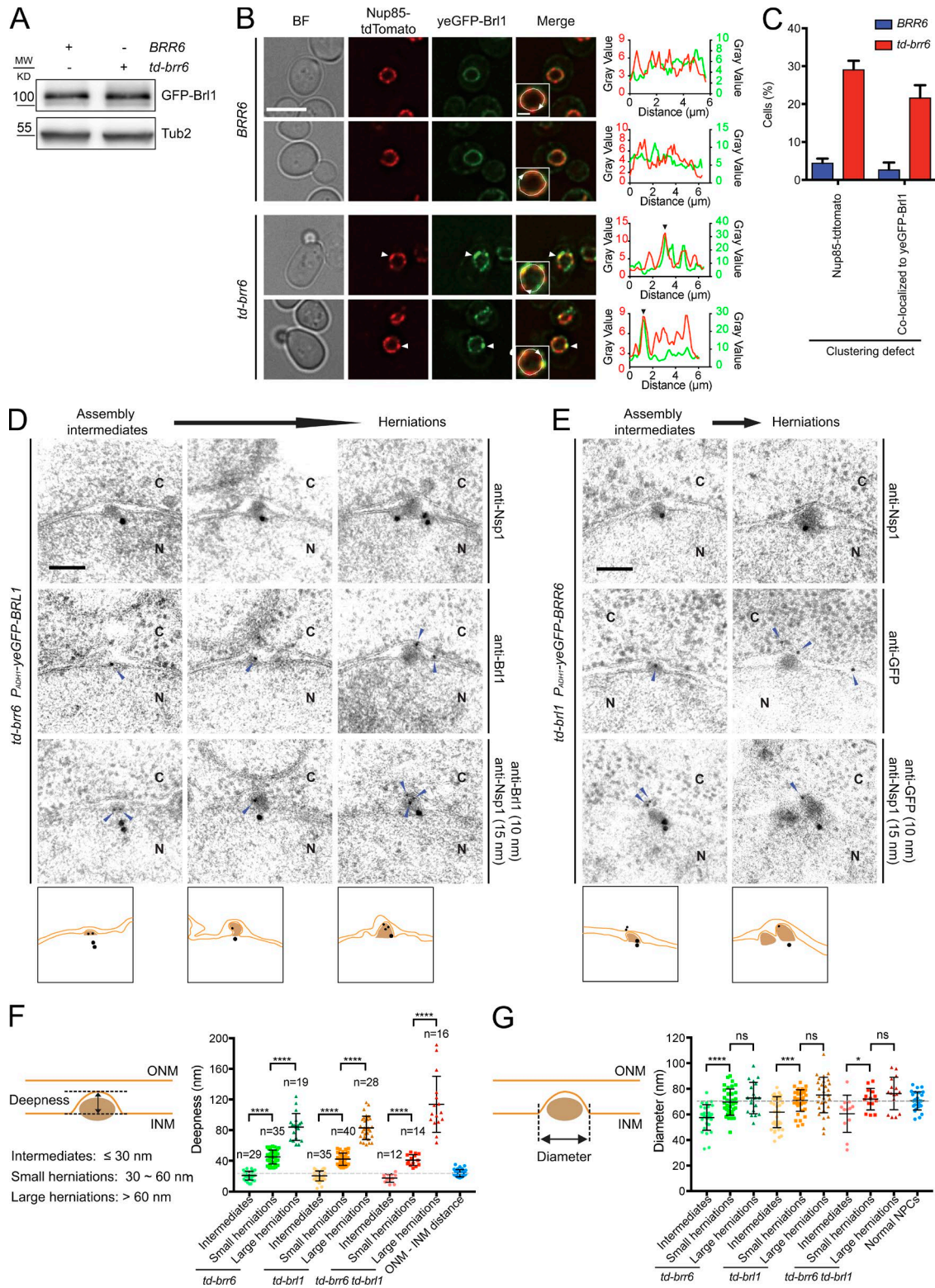
Figure 8. **Brr6 and Brl1 accumulate at NPC assembly intermediates.** **(A)** Protein level of yeGFP-Brl1 of the indicated cells represented in B. Tub2 is loading control. **(B)** Images of cells incubated at 37°C for 3 h. The enlargements (bottom) show NEs that were used for the plot profiles (right). Arrowheads indicate colocalization of yeGFP-Brl1 and Nup85-tdTomato. Bars: (overview) 5 µm; (enlargement) 1 µm. **(C)** Quantification of cells from B. Error bars: SD (n > 230); three independent experiments. **(D and E)** Immuno-EM of cells incubated for 3 h at 37°C. Localization of Brl1, Brr6 (10 nm gold, anti-Brl1, and anti-GFP), and Nsp1 (15 nm, anti-Nsp1) at NPC intermediates and herniations. Cartoons illustrate the morphology of the NE evaginations with gold labeling. N, nucleus; C, cytoplasm. Bars, 100 nm. **(F)** Deepness of NPC intermediates and herniations of Nsp1-labeled cells was measured as indicated by the bidirectional arrows in the cartoon. ONM–INM distance was measured from *BRR6 BRL1* WT cells near NPCs. ****, P ≤ 0.0001. **(G)** Diameter of NPC intermediates and herniations (see cartoon) was quantified from *td-brr6*, *td-brl1*, and *td-brr6 td-brl1* cells. The diameter of normal NPCs was measured from *BRR6 BRL1* WT cells. *, P ≤ 0.05; ***, P ≤ 0.001; ****, P ≤ 0.0001; ns, not significant.

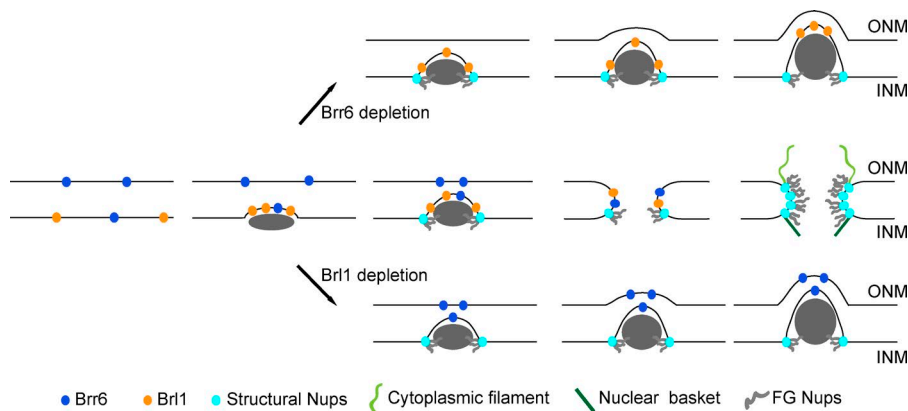Figure 9. **Model for Brr6/Brl1 function.** See Discussion for details.

Legend: ● Brr6 ● Brl1 ● Structural Nups (Cytoplasmic filament \ Nuclear basket ⌇ FG Nups

and fusion (Thiam et al., 2013; McMahon and Boucrot, 2015). In addition, BA affected growth of only a subset of conditional lethal *brl1* mutant cells, although all of them showed NPC biogenesis defects. *brr6-5001* cells grew even better on BA at 33°C than without the drug. BA also impaired growth of well-studied SPB duplication and NPC biogenesis mutants that are important for the insertion of the SPB or NPC into the NE but are not involved in lipid biogenesis. Thus, a change in growth by BA probably indicates a role of the encoded protein in membrane-related processes but does not necessarily indicate a function in lipid homeostasis.

Previously it was suggested that the C terminus of Brr6 is in the intermembrane space of the NE, whereas the N terminus is exposed into the nucleo- or cytoplasm (de Bruyn Kops and Guthrie, 2001). Our data are most consistent with the model that Brr6 and Brl1 have two TM domains with N and C termini exposed to the nucleoplasm or cytoplasm (Fig. 4 J). In agreement with this model are membrane orientation predications (Kim et al., 2006; Smoyer et al., 2016) and the observation that N and C termini of Brl1 interact in the split YFP assay, indicating that they colocalize on the same side of the NE. Similarly, N- and C-tagged Brr6 interacted with Brl1 in the BiFC. Furthermore, the HBH tag at the N terminus of Brl1 and N and C termini of Brr6 was found to be biotinylated by endogenous biotin transferase, which resides in the nucleus and cytoplasm but not in the ER lumen. In addition, Brr6 and Brl1 formed intramolecular disulfide bonds, most likely inside the oxidative environment of the intermembrane space of the NE. The two most inner cysteine residues of Brl1 were essential for its function. We propose that disulfide bond formation within the intermembrane space is important to stabilize the fold of Brl1, which then has an impact on the membrane insertion, localization, and stability of the protein.

How do Brr6 and Brl1 function in NPC biogenesis? Recent data indicate that the GLFG repeats of Nup116 not only have a NPC transport function, but in addition play a role in NPC biogenesis by stabilizing critical interactions with scaffold NUPs during interphase NPC biogenesis. Failure of this stabilization causes NPC biogenesis defects, with the accumulation of herniations (Onischenko et al., 2017). Herniations are also a prominent phenotype of *brr6(ts)* and *brl1(ts)* mutant cells (Hodge et al., 2010; Lone et al., 2015). Puzzlingly, however, Brr6 and Brl1 do not colocalize with clustered NPCs in *nup133Δ* cells, leading to the suggestion that they are not associated with NPCs (de Bruyn Kops and Guthrie, 2001; Saitoh et al., 2005). Immuno-EM data presented here indicate that Brr6 and Brl1 interact with a subset of NPCs. These may be newly assembled NPCs

or a specific subset of already assembled NPCs. In addition, Brr6 and Brl1 localized to INM evaginations of NPC assembly intermediates that are morphologically related to the NPC assembly intermediates in human cells (Otsuka et al., 2016). Furthermore, Brr6 and Brl1 were essential for the biogenesis of new NPCs. Mature NPCs were not affected by the depletion of both proteins. Clustering of Brr6 and Brl1 at the NE was sufficient to recruit the NPC component Nup188. This altogether supports the notion that Brr6 and Brl1 transiently interact with assembling NPCs (Fig. 9).

Brr6 and Brl1 could be part of a control mechanism that repairs defective or stalled assembly intermediates, as was shown recently for Heh2 and the AAA-ATPase Vps4 (Webster et al., 2014). We consider this possibility as less likely, because in cells lacking the repair pathway genes *HEH2* or *VPS4*, NPC assembly defects are relatively rare even in the absence of *POM152* and *VPS4* (<15%; Webster et al., 2014). Thus, NPC biogenesis is highly efficient even without a repair pathway. In contrast, only 1-h depletion of Brr6 and Brl1 affected ∼50% of the newly assembled NPCs (Fig. 1 E), and depletion of Brr6/Brl1 for 3 h impaired most of the NPCs (Fig. 1, B and C; and Fig. S1, D and E). This strong NPC biogenesis defect is more in line with a function of Brr6 and Brl1 in the assembly of new NPCs. We favor a model in which Brl1 either scaffolds NPC assembly independent of Nup188 and GLFG-Nup116 or promotes fusion of the INM and ONM by remodeling the NE during NPC biogenesis. This model is consistent with the observation that *BRL1* overexpression was able to bypass the functions of *NUP116* and *GLE2* in NPC biogenesis. In fact, the INM evagination phenotype of *nup116Δ* and *gle2Δ* cells was completely suppressed by P_{ADH1}-*BRL1*. Furthermore, P_{ADH1}-*BRL1* suppressed the growth defect of *nup116ΔGLFG* P_{MET3}-*NUP188* cells that arises because of a lack of scaffold function during NPC biogenesis (Onischenko et al., 2017). Future in vitro experiments will test whether purified Brl1 has membrane-remodeling activity.

Complex formation, genetic interactions, and similar phenotypes of conditional lethal mutants suggest that Brr6 and Brl1 function together in one complex. However, it is important to note that Brr6 does not always behave like Brl1. In contrast to *BRL1*, overexpression of *BRR6* failed to suppress the growth defect of *nup116(ts)* and *gle2(ts)* cells and did not affect NE morphology. Moreover, about half of Brr6 associated with the ONM, whereas most of Brl1 was at the INM. This may indicate that Brr6 and Brl1 do not always function together. It will be important to understand when in the NPC biogenesis process both proteins interact and which functions of *BRL1* require *BRR6*.

The *S. pombe* Brr6 becomes enriched at the SPB in early mitosis and with mitotic exit, where it facilitates NE insertion and extrusion of the SPB from the NE, respectively (Tamm et al., 2011). Such function at the SPB was not obvious in *S. cerevisiae*. We detected only relatively mild SPB duplication defects that could be an indirect consequence of the NPC defects in Brr6/Brl1-depleted cells (Rüthnick et al., 2017). We were unable to show enrichment of Brr6 and Brl1 at the SPB of budding yeast. The difference between *S. pombe* and *S. cerevisiae* is probably an attribute of distinct SPB insertion mechanisms (Cavanaugh and Jaspersen, 2017). In *S. cerevisiae*, the daughter SPB inserts next to the mother SPB that is already embedded in the NE (Seybold and Schiebel, 2013). In *S. pombe*, the mother and daughter SPBs reside on the cytoplasmic face of the NE during interphase, and both become inserted into a fenestra of the NE with mitotic entry (Ding et al., 1997; Bouhlel et al., 2015; Rüthnick and Schiebel, 2016).

In mammalian cells, the membrane curvature–sensing protein Nup133, the Sun domain protein Sun1, and the TM NUP Pom121 have been reported to be involved in interphase NPC assembly (Doucet et al., 2010; Funakoshi et al., 2011; Talamas and Hetzer, 2011). Puzzlingly, Brr6/Brl1 homologues are found only in organisms with closed mitosis (Tamm et al., 2011; Jaspersen and Ghosh, 2012; Yang et al., 2017). In these organisms, the interphase NPC pathway is probably the only way to assemble NPCs and as such has to be particularly efficient. This may explain the conservation of Brr6/Brl1 in these organisms. Functionally similar proteins most likely fulfill the role of Brr6/Brl1 in interphase NPC biogenesis in higher eukaryotes. It will be interesting to test the extended reticulon family (Yang and Strittmatter, 2007; Christodoulou et al., 2016) and Torsin, whose depletion causes accumulation of herniation-like structures in human cells (Laudermilch et al., 2016), for functions in INM-ONM fusion during interphase NPC biogenesis.

Materials and methods

Yeast strains and culture conditions
Yeast strains and plasmids used in this study are listed in Table S1. Yeast strains TSA1123, Y12346, and Y12360 were obtained from C. Boone (Donnelly Centre for Cellular and Biomolecular Research, University of Toronto, Toronto, Canada). The plasmids pUN100-SEC13-ProtA and pUN100-sec13-34-ProtA were obtained from E. Hurt (Heidelberg University Biochemistry Center, Heidelberg, Germany). The plasmid pLPMR2 was obtained from C.P. Lusk (Yale School of Medicine, New Haven, CT). The yeast strain ScEB116 was obtained from G. Rabut (Centre National de la Recherche Scientifique, Rennes, France). The yeast strain KWY5540 was obtained from K. Weis (Institut für Biochemie, ETH Zurich, Zurich, Switzerland). The yeast strain SWY1136 was obtained from S. Wente (Vanderbilt University School of Medicine, Nashville, TN). Gene deletion and epitope tagging of endogenous genes were performed using a PCR-based integration approach (Knop et al., 1999; Janke et al., 2004). Yeast strains were grown in synthetic complete (SC) medium, SC-selection medium (Rose, 1987), YPD, or yeast extract, peptone, and raffinose (YPRaf) with or without 0.1 mM $CuSO_4$ at 16°C, 23°C, 30°C, or 37°C. Galactose was added to a final concentration of 2% to induce expression of genes under a *GAL1* promoter. Alkaline lysis and TCA precipitation were used to prepare yeast extracts for analysis of protein levels by immunoblotting (Janke et al., 2004). To test for growth defects, yeast cells were grown overnight in the indicated selection medium before the density was adjusted to $OD_{600} = 1$ the next day. The cell suspension was then spotted in a 10-fold serial dilution on the desired plates and incubated at the indicated temperatures.

Fluorescence light microscopy
A DeltaVision RT system (Olympus IX71 based; Applied Precision) equipped with the Photometrics CoolSnap HQ camera (Roper Scientific), a 100×/1.4-NA UPlanSAPO objective (Olympus), a mercury arc light source, and softWoRx software (Applied Precision) was used for cell imaging. Imaging was done at 23°C, 30°C, or 37°C using the GFP, YFP, and mCherry channels with different exposure times according to the fluorescence intensity of each protein. For time-lapse experiments, cells were grown and imaged in microfluidic plates (Y04C/CellASIC) within the ONIX microfluidic platform (CellASIC) inserted onto the microscope stage. SC medium with 3% raffinose and 2% galactose was perfused into the microfluidic plate at a pressure of 0.25 psi. Image restoration by 3D deconvolution was performed with softWoRx and processed with ImageJ software (National Institutes of Health). For quantification of SPB signals, the integrated density (IntDen) of the SPB in the brightest stack was measured with a 5 × 5-pixel square and 7 × 7-pixel square for background correction. The following formula was used to calculate the relative fluorescent intensity (RFI):

$$RFI = IntDen_{5\times5} - \{(IntDen_{7\times7} - IntDen_{5\times5}) \times [area_{5\times5}/(area_{7\times7} - area_{5\times5})]\}.$$

Quantifications were performed three times, and a combined graph is shown.

Lipid analysis
Cells (10 OD) were harvested and homogenized by FastPrep (MP Biomedicals) in 155-mM ammonium bicarbonate buffer (pH 7.5). Homogenized cells were subjected to acidic Bligh–Dyer lipid extraction in the presence of internal lipid standards added from a master mix containing phosphatidylcholine (PC; 13:0/13:0, 14:0/14:0, 20:0/20:0; 21:0/21:0; Avanti Polar Lipids), phosphatidylinositol (PI; 17:0/20:4; Avanti Polar Lipids), phosphatidylethanolamine and phosphatidylserine (PE and PS; both 14:1/14:1, 20:1/20:1, 22:1/22:1; semisynthesized as described in Özbalci et al. [2013]), DAG (17:0/17:0; Larodan), TAG (TAG, D5-TAG-Mix, and LM-6000/D5-TAG, 17:0, 17:1, and 17:1; Avanti Polar Lipids), phosphatidic acid (PA, 17:0/20:4; Avanti Polar Lipids), phosphatidylglycerol (PG, 14:1/14:1, 20:1/20:1, 22:1/22:1; semisynthesized as described in Özbalci et al. [2013]), and t-ceramide (t-Cer; Avanti Polar Lipids). Lipids recovered in the organic extraction phase were evaporated by a gentle stream of nitrogen. Before measurements, lipid extracts were dissolved in 10 mM ammonium acetate in methanol and transferred to 96-well plates (Eppendorf Twintec 96). Mass spectrometry measurements were performed in positive ion mode on an AB SCIEX QTRAP 6500+ mass spectrometer, equipped with chip-based (HD-D ESI Chip; Advion Biosciences) nano-electrospray infusion, and ionization (Triversa Nanomate; Advion Biosciences) as described previously (Özbalci et al., 2013). The following precursor ion scanning (PREC) and neutral loss scanning (NL) modes were used for the measurement of the various lipid classes: +PREC 184 (PC), +PREC282 (t-Cer), +NL141 (PE), +NL185 (PS), +NL277 (PI), +NL189 (PG), +NL115 (PA), and +PREC 77 (ergosterol). Ergosterol was quantified after derivatization to ergosterol acetate in the presence of the internal standard (22E)-Stigmasta-5,7,22-trien-3-β-ol (R202967; Sigma-Aldrich) using 100 µl acetic anhydride/chloroform (1:12 vol/vol; Ejsing et al., 2009). Data evaluation was done using LipidView (ABSciex) and an in-house–developed software (ShinyLipids).

Bimolecular fluorescence complementation

The BiFC interaction assay was performed using Brl1 and NUPs tagged with either VC173 or VN155 fragments (VC and VN) of the Venus fluorescent protein (Shyu et al., 2006). All fusions were expressed from their endogenous chromosomal loci. The strains expressing *BRL1-VC* were constructed on the scEB116 background, and NUPs-VN were constructed by homologous recombination in the BY4741 background. Strains expressing individual *BRL1-VC* and *NUPs-VN* fusions were mated to produce an array of yeast strains each expressing a unique combination of tagged *BRL1* and NUP, as described previously (Baryshnikova et al., 2010). The resulting strains were cultivated overnight at 30°C in SC medium and diluted in SC medium again for 3–4 h at 30°C or 16–18 h at 16°C before imaging.

Redox-state detection via alkylation shift experiments

To analyze the redox state of cysteine residues in Brr6 and Brl1 in vivo, cells were grown in YPD medium to exponential phase, followed by treatment with or without 50 mM NEM. The whole-cell lysates were TCA precipitated with the modified protocol as described previously (Keogh et al., 2006). In brief, cells at 3 OD were resuspended in 250 µl of 20% TCA and subjected to glass bead lysis. The precipitated proteins were washed with 1 ml ice-cold acetone and dissolved in modification buffer (Ramesh et al., 2016) with or without 10 mM TCEP for 20 min at 96°C. The resuspensions were modified with 15 mM mmPEG24 for 2 h in the dark.

Immunoprecipitation

Cells (25 OD) were harvested and resuspended in lysis buffer (20 mM Tris-Cl, pH 8.0, 150 mM NaCl, 5 mM MgCl$_2$, and 10% glycerol) supplemented with 10 mM NaF, 60 mM β-glycerophosphate, 1 tablet/50 ml Roche protease inhibitor cocktail complete (EDTA free), and 1 mM PMSF. Glass beads (BioSpec Products) were added, and cells were lysed in a FastPrep machine (MP Biomedicals). Cell lysate was supplemented with 0.5% Triton X-100 and incubated on ice for 10 min. The soluble proteins were separated from the cell debris by centrifugation and incubated with GFP-Trap agarose beads (Chromotek) at 4°C for 2 h. Beads were washed three times with lysis buffer supplemented with 0.1% Triton X-100 and twice with wash buffer (20 mM Tris-Cl, pH 8.0, 150 mM NaCl, and 5 mM MgCl$_2$). Bound proteins were eluted in 50 µl of 2× SDS-PAGE sample buffer, heated to 95°C for 5 min, separated by SDS-PAGE, and transferred to PVDF membrane (Millipore) for Western blotting.

EM

Cells were high-pressure frozen, freeze-substituted, sectioned, labeled, and stained for EM. In brief, cells were collected onto a 0.45-µm polycarbonate filter (Millipore) using vacuum filtration and high-pressure frozen with a HPM010 (Abra-Fluid). Cells were freeze-substituted (freeze substitution solution: 0.1% glutaraldehyde, 0.2% uranyl acetate, and 1% water, dissolved in anhydrous acetone) using the EM-AFS2 device (Leica Microsystems) and stepwise infiltrated with Lowicryl HM20 (Polysciences), started by a low temperature of −90°C. For polymerization, the samples were finally exposed to UV light for 48 h at −45°C and were gradually warmed up to 20°C. Embedded cells were serially sectioned using a Reichert Ultracut S Microtome (Leica Instruments) to a thickness of 70 nm. Poststaining with 3% uranyl acetate and lead citrate was performed. The sections were imaged on a CM120 BioTwin electron microscope (Philips Electronics) operated at 80–100 kV and equipped with a CCD camera (Keen View; Soft Imaging Systems) or a JE-1400 (Jeol) operating at 80 kV equipped with a 4,000 × 4,000 digital camera (F416; TVIPS). Micrographs were adjusted in brightness and contrast using ImageJ. For immunolabeling, primary antibodies were used against GFP, Brl1, and Nsp1. The samples were prepared similarly, with the exception that the glutaraldehyde was omitted from the freeze-substitution solution. The sections were treated with blocking buffer (1.5% BSA and 0.1% fish skin gelatin in PBS), then incubated with the primary antibodies, followed by treatment with protein A–gold conjugates (10 nm, Utrecht University). For double immunolabeling, after incubation with the mixture of primary antibodies, the sections were treated with anti–rabbit gold (10 nm) and anti–mouse gold (15 nm) conjugates. The following formula was used to calculate NPC occupancy: NPC occupancy = (number of NPC × average of NPC diameter)/length of NE. The average NPC diameter was calculated to be 70 nm from Fig. 8 G. Quantifications were performed in 48 cells.

Statistical analysis

For the statistical analyses, PRISM v.7 software (GraphPad) was used. Comparisons of samples were performed using unpaired *t* test with two-tailed p-value. Data distribution was assumed to be normal, but this was not formally tested.

Antibodies

Antibodies and their conditions of use are as follows: mouse anti-Nsp1 (immuno-EM, 1:100; ab4641; Abcam), rabbit anti-GFP (immuno-EM, 1:5; gift from M. Seedorf, Zentrum für Molekulare Biologie, Heidelberg, Germany), mouse anti-GFP (Western blot, 1:1,000; 11814460 001; Roche), rabbit anti-Brl1 (immuno-EM, 1:5; Western blot, 1:50; made in-house), mouse anti-His (Western blot, 1:1,000; 34660; Qiagen), rabbit anti-Tub2 (Western blot, 1:1,000; made in-house), and mouse anti-HA (Western blot, 1:100, made in-house).

Online supplemental material

Fig. S1 describes that NPC biogenesis is affected in *td-brr6 td-brl1* cells, associated with Fig. 1. Fig. S2 provides information regarding SPB duplication defects in *td-brr6 td-brl1* cells. It also describes the localization of Brr6 and Brl1 during the cell cycle with Spc42 as a SPB marker. Fig. S3 shows that mutations in conserved cysteine residues cause mislocalization or destabilization of Brl1, and that NE localization of Nup188-mCherry by 3GBP expression is not affected in *OLE1-3GFP* cells. Fig. S4 shows that overexpression of *BRL1* promotes formation of NE sheets inside the nucleus. Table S1 shows yeast strains used in this study.

References

Alber, F., S. Dokudovskaya, L.M. Veenhoff, W. Zhang, J. Kipper, D. Devos, A. Suprapto, O. Karni-Schmidt, R. Williams, B.T. Chait, et al. 2007. The molecular architecture of the nuclear pore complex. *Nature.* 450:695–701. https://doi.org/10.1038/nature06405

Baryshnikova, A., M. Costanzo, S. Dixon, F.J. Vizeacoumar, C.L. Myers, B. Andrews, and C. Boone. 2010. Synthetic genetic array (SGA) analysis in Saccharomyces cerevisiae and Schizosaccharomyces pombe. *Methods Enzymol.* 470:145–179. https://doi.org/10.1016/S0076-6879(10)70007-0

Beck, M., and E. Hurt. 2017. The nuclear pore complex: Understanding its function through structural insight. *Nat. Rev. Mol. Cell Biol.* 18:73–89. https://doi.org/10.1038/nrm.2016.147

Bouhlel, I.B., M. Ohta, A. Mayeux, N. Bordes, F. Dingli, J. Boulanger, G. Velve Casquillas, D. Loew, P.T. Tran, M. Sato, and A. Paoletti. 2015. Cell cycle control of spindle pole body duplication and splitting by Sfi1 and Cdc31 in fission yeast. *J. Cell Sci.* 128:1481–1493. https://doi.org/10.1242/jcs.159657

Braakman, I., H. Hoover-Litty, K.R. Wagner, and A. Helenius. 1991. Folding of influenza hemagglutinin in the endoplasmic reticulum. *J. Cell Biol.* 114:401–411. https://doi.org/10.1083/jcb.114.3.401

Cavanaugh, A.M., and S.L. Jaspersen. 2017. Big lessons from little yeast: Budding and fission yeast centrosome structure, duplication, and function. *Annu. Rev. Genet.* 51:361–383. https://doi.org/10.1146/annurev-genet-120116-024733

Chial, H.J., M.P. Rout, T.H. Giddings, and M. Winey. 1998. *Saccharomyces cerevisiae* Ndc1p is a shared component of nuclear pore complexes and spindle pole bodies. *J. Cell Biol.* 143:1789–1800. https://doi.org/10.1083/jcb.143.7.1789

Christodoulou, A., R. Santarella-Mellwig, N. Santama, and I.W. Mattaj. 2016. Transmembrane protein TMEM170A is a newly discovered regulator of ER and nuclear envelope morphogenesis in human cells. *J. Cell Sci.* 129:1552–1565. https://doi.org/10.1242/jcs.175273

de Bruyn Kops, A., and C. Guthrie. 2001. An essential nuclear envelope integral membrane protein, Brr6p, required for nuclear transport. *EMBO J.* 20:4183–4193. https://doi.org/10.1093/emboj/20.15.4183

Delic, M., M. Valli, A.B. Graf, M. Pfeffer, D. Mattanovich, and B. Gasser. 2013. The secretory pathway: Exploring yeast diversity. *FEMS Microbiol. Rev.* 37:872–914. https://doi.org/10.1111/1574-6976.12020

Ding, R., R.R. West, D.M. Morphew, B.R. Oakley, and J.R. McIntosh. 1997. The spindle pole body of Schizosaccharomyces pombe enters and leaves the nuclear envelope as the cell cycle proceeds. *Mol. Biol. Cell.* 8:1461–1479. https://doi.org/10.1091/mbc.8.8.1461

Doucet, C.M., J.A. Talamas, and M.W. Hetzer. 2010. Cell cycle-dependent differences in nuclear pore complex assembly in metazoa. *Cell.* 141:1030–1041. https://doi.org/10.1016/j.cell.2010.04.036

Eibauer, M., M. Pellanda, Y. Turgay, A. Dubrovsky, A. Wild, and O. Medalia. 2015. Structure and gating of the nuclear pore complex. *Nat. Commun.* 6:7532. https://doi.org/10.1038/ncomms8532

Ejsing, C.S., J.L. Sampaio, V. Surendranath, E. Duchoslav, K. Ekroos, R.W. Klemm, K. Simons, and A. Shevchenko. 2009. Global analysis of the yeast lipidome by quantitative shotgun mass spectrometry. *Proc. Natl. Acad. Sci. USA.* 106:2136–2141. https://doi.org/10.1073/pnas.0811700106

Emerman, A.B., Z.R. Zhang, O. Chakrabarti, and R.S. Hegde. 2010. Compartment-restricted biotinylation reveals novel features of prion protein metabolism in vivo. *Mol. Biol. Cell.* 21:4325–4337. https://doi.org/10.1091/mbc.E10-09-0742

Frand, A.R., J.W. Cuozzo, and C.A. Kaiser. 2000. Pathways for protein disulphide bond formation. *Trends Cell Biol.* 10:203–210. https://doi.org/10.1016/S0962-8924(00)01745-1

Funakoshi, T., M. Clever, A. Watanabe, and N. Imamoto. 2011. Localization of Pom121 to the inner nuclear membrane is required for an early step of interphase nuclear pore complex assembly. *Mol. Biol. Cell.* 22:1058–1069. https://doi.org/10.1091/mbc.E10-07-0641

Gerace, L., Y. Ottaviano, and C. Kondor-Koch. 1982. Identification of a major polypeptide of the nuclear pore complex. *J. Cell Biol.* 95:826–837. https://doi.org/10.1083/jcb.95.3.826

Gillespie, P.J., G.A. Khoudoli, G. Stewart, J.R. Swedlow, and J.J. Blow. 2007. ELYS/MEL-28 chromatin association coordinates nuclear pore complex assembly and replication licensing. *Curr. Biol.* 17:1657–1662. https://doi.org/10.1016/j.cub.2007.08.041

Hallberg, E., R.W. Wozniak, and G. Blobel. 1993. An integral membrane protein of the pore membrane domain of the nuclear envelope contains a nucleoporin-like region. *J. Cell Biol.* 122:513–521. https://doi.org/10.1083/jcb.122.3.513

Hetzer, M.W., and S.R. Wente. 2009. Border control at the nucleus: Biogenesis and organization of the nuclear membrane and pore complexes. *Dev. Cell.* 17:606–616. https://doi.org/10.1016/j.devcel.2009.10.007

Hodge, C.A., V. Choudhary, M.J. Wolyniak, J.J. Scarcelli, R. Schneiter, and C.N. Cole. 2010. Integral membrane proteins Brr6 and Apq12 link assembly of the nuclear pore complex to lipid homeostasis in the endoplasmic reticulum. *J. Cell Sci.* 123:141–151. https://doi.org/10.1242/jcs.055046

Hu, C.D., Y. Chinenov, and T.K. Kerppola. 2002. Visualization of interactions among bZIP and Rel family proteins in living cells using bimolecular fluorescence complementation. *Mol. Cell.* 9:789–798. https://doi.org/10.1016/S1097-2765(02)00496-3

Huh, W.K., J.V. Falvo, L.C. Gerke, A.S. Carroll, R.W. Howson, J.S. Weissman, and E.K. O'Shea. 2003. Global analysis of protein localization in budding yeast. *Nature.* 425:686–691. https://doi.org/10.1038/nature02026

Janke, C., M.M. Magiera, N. Rathfelder, C. Taxis, S. Reber, H. Maekawa, A. Moreno-Borchart, G. Doenges, E. Schwob, E. Schiebel, and M. Knop. 2004. A versatile toolbox for PCR-based tagging of yeast genes: New fluorescent proteins, more markers and promoter substitution cassettes. *Yeast.* 21:947–962. https://doi.org/10.1002/yea.1142

Jaspersen, S.L., and S. Ghosh. 2012. Nuclear envelope insertion of spindle pole bodies and nuclear pore complexes. *Nucleus.* 3:226–236. https://doi.org/10.4161/nucl.20148

Kanemaki, M., A. Sanchez-Diaz, A. Gambus, and K. Labib. 2003. Functional proteomic identification of DNA replication proteins by induced proteolysis in vivo. *Nature.* 423:720–724. https://doi.org/10.1038/nature01692

Keogh, M.C., J.A. Kim, M. Downey, J. Fillingham, D. Chowdhury, J.C. Harrison, M. Onishi, N. Datta, S. Galicia, A. Emili, et al. 2006. A phosphatase complex that dephosphorylates gamma H2AX regulates DNA damage checkpoint recovery. *Nature.* 441:120. https://doi.org/10.1038/nature04772

Kerppola, T.K. 2008. Bimolecular fluorescence complementation: Visualization of molecular interactions in living cells. *Methods Cell Biol.* 85:431–470. https://doi.org/10.1016/S0091-679X(08)85019-4

Khmelinskii, A., P.J. Keller, H. Lorenz, E. Schiebel, and M. Knop. 2010. Segregation of yeast nuclear pores. *Nature.* 466:E1. https://doi.org/10.1038/nature09255

Khmelinskii, A., E. Blaszczak, M. Pantazopoulou, B. Fischer, D.J. Omnus, G. Le Dez, A. Brossard, A. Gunnarsson, J.D. Barry, M. Meurer, et al. 2014. Protein quality control at the inner nuclear membrane. *Nature.* 516:410–413. https://doi.org/10.1038/nature14096

Kim, H., K. Melén, M. Osterberg, and G. von Heijne. 2006. A global topology map of the Saccharomyces cerevisiae membrane proteome. *Proc. Natl. Acad. Sci. USA.* 103:11142–11147. https://doi.org/10.1073/pnas.0604075103

Knop, M., K. Siegers, G. Pereira, W. Zachariae, B. Winsor, K. Nasmyth, and E. Schiebel. 1999. Epitope tagging of yeast genes using a PCR-based strategy: More tags and improved practical routines. *Yeast.* 15(10B):963–972. https://doi.org/10.1002/(SICI)1097-0061(199907)15:10B<963::AID-YEA399>3.0.CO;2-W

Laudermilch, E., P.L. Tsai, M. Graham, E. Turner, C. Zhao, and C. Schlieker. 2016. Dissecting Torsin/cofactor function at the nuclear envelope: A genetic study. *Mol. Biol. Cell.* 27:3964–3971. https://doi.org/10.1091/mbc.E16-07-0511

Liu, G., M.Y. Yong, M. Yurieva, K.G. Srinivasan, J. Liu, J.S. Lim, M. Poidinger, G.D. Wright, F. Zolezzi, H. Choi, et al. 2015. Gene essentiality is a quantitative property linked to cellular evolvability. *Cell.* 163:1388–1399. https://doi.org/10.1016/j.cell.2015.10.069

Loïodice, I., A. Alves, G. Rabut, M. Van Overbeek, J. Ellenberg, J.B. Sibarita, and V. Doye. 2004. The entire Nup107-160 complex, including three new members, is targeted as one entity to kinetochores in mitosis. *Mol. Biol. Cell.* 15:3333–3344. https://doi.org/10.1091/mbc.E03-12-0878

Lone, M.A., A.E. Atkinson, C.A. Hodge, S. Cottier, F. Martínez-Montañés, S. Maithel, L. Mène-Saffrané, C.N. Cole, and R. Schneiter. 2015. Yeast integral membrane proteins Apq12, Brl1, and Brr6 form a complex important for regulation of membrane homeostasis and nuclear pore complex biogenesis. *Eukaryot. Cell.* 14:1217–1227. https://doi.org/10.1128/EC.00101-15

Lutzmann, M., R. Kunze, K. Stangl, P. Stelter, K.F. Tóth, B. Böttcher, and E. Hurt. 2005. Reconstitution of Nup157 and Nup145N into the Nup84 complex. *J. Biol. Chem.* 280:18442–18451. https://doi.org/10.1074/jbc.M412787200

McMahon, H.T., and E. Boucrot. 2015. Membrane curvature at a glance. *J. Cell Sci.* 128:1065–1070. https://doi.org/10.1242/jcs.114454

Miao, M., K.J. Ryan, and S.R. Wente. 2006. The integral membrane protein Pom34p functionally links nucleoporin subcomplexes. *Genetics.* 172:1441–1457. https://doi.org/10.1534/genetics.105.052068

Mukhopadhyay, K., A. Kohli, and R. Prasad. 2002. Drug susceptibilities of yeast cells are affected by membrane lipid composition. *Antimicrob. Agents Chemother.* 46:3695–3705. https://doi.org/10.1128/AAC.46.12.3695 -3705.2002

Murphy, R., J.L. Watkins, and S.R. Wente. 1996. GLE2, a Saccharomyces cerevisiae homologue of the Schizosaccharomyces pombe export factor RAE1, is required for nuclear pore complex structure and function. *Mol. Biol. Cell.* 7:1921–1937. https://doi.org/10.1091/mbc.7.12.1921

Onischenko, E., J.H. Tang, K.R. Andersen, K.E. Knockenhauer, P. Vallotton, C.P. Derrer, A. Kralt, C.F. Mugler, L.Y. Chan, T.U. Schwartz, and K. Weis. 2017. Natively unfolded FG repeats stabilize the structure of the nuclear pore complex. *Cell.* 171:904–917. https://doi.org/10.1016/j .cell.2017.09.033

Otsuka, S., K.H. Bui, M. Schorb, M.J. Hossain, A.Z. Politi, B. Koch, M. Eltsov, M. Beck, and J. Ellenberg. 2016. Nuclear pore assembly proceeds by an inside-out extrusion of the nuclear envelope. *eLife.* 5:e19071. https://doi .org/10.7554/eLife.19071

Özbalci, C., T. Sachsenheimer, and B. Brügger. 2013. Quantitative analysis of cellular lipids by nano-electrospray ionization mass spectrometry. *Methods Mol. Biol.* 1033:3–20. https://doi.org/10.1007/978-1-62703-487 -6_1

Radu, A., M.S. Moore, and G. Blobel. 1995. The peptide repeat domain of nucleoporin Nup98 functions as a docking site in transport across the nuclear pore complex. *Cell.* 81:215–222. https://doi.org/10.1016/0092 -8674(95)90331-3

Ramesh, A., V. Peleh, S. Martinez-Caballero, F. Wollweber, F. Sommer, M. van der Laan, M. Schroda, R.T. Alexander, M.L. Campo, and J.M. Herrmann. 2016. A disulfide bond in the TIM23 complex is crucial for voltage gating and mitochondrial protein import. *J. Cell Biol.* 214:417–431. https://doi .org/10.1083/jcb.201602074

Rexach, M. 2009. Piecing together nuclear pore complex assembly during interphase. *J. Cell Biol.* 185:377–379. https://doi.org/10.1083/jcb .200904022

Rose, M.D. 1987. Isolation of genes by complementation in yeast. *Methods Enzymol.* 152:481–504. https://doi.org/10.1016/0076-6879(87)52056-0

Rothbauer, U., K. Zolghadr, S. Muyldermans, A. Schepers, M.C. Cardoso, and H. Leonhardt. 2008. A versatile nanotrap for biochemical and functional studies with fluorescent fusion proteins. *Mol. Cell. Proteomics.* 7:282–289. https://doi.org/10.1074/mcp.M700342-MCP200

Rüthnick, D., and E. Schiebel. 2016. Duplication of the yeast spindle pole body once per cell cycle. *Mol. Cell. Biol.* 36:1324–1331. https://doi.org/10 .1128/MCB.00048-16

Rüthnick, D., A. Neuner, F. Dietrich, D. Kirrmaier, U. Engel, M. Knop, and E. Schiebel. 2017. Characterization of spindle pole body duplication reveals a regulatory role for nuclear pore complexes. *J. Cell Biol.* 216:2425–2442. https://doi.org/10.1083/jcb.201612129

Saitoh, Y.H., K. Ogawa, and T. Nishimoto. 2005. Brl1p—A novel nuclear envelope protein required for nuclear transport. *Traffic.* 6:502–517. https ://doi.org/10.1111/j.1600-0854.2005.00295.x

Schneiter, R., and C.N. Cole. 2010. Integrating complex functions: Coordination of nuclear pore complex assembly and membrane expansion of the nuclear envelope requires a family of integral membrane proteins. *Nucleus.* 1:387–392. https://doi.org/10.4161/nucl.1.5.12333

Seybold, C., and E. Schiebel. 2013. Spindle pole bodies. *Curr. Biol.* 23:R858–R860. https://doi.org/10.1016/j.cub.2013.07.024

Shyu, Y.J., H. Liu, X. Deng, and C.D. Hu. 2006. Identification of new fluorescent protein fragments for bimolecular fluorescence complementation analysis under physiological conditions. *Biotechniques.* 40:61–66. https://doi.org /10.2144/000112036

Siniossoglou, S., M. Lutzmann, H. Santos-Rosa, K. Leonard, S. Mueller, U. Aebi, and E. Hurt. 2000. Structure and assembly of the Nup84p complex. *J. Cell Biol.* 149:41–54. https://doi.org/10.1083/jcb.149.1.41

Smoyer, C.J., S.S. Katta, J.M. Gardner, L. Stoltz, S. McCroskey, W.D. Bradford, M. McClain, S.E. Smith, B.D. Slaughter, J.R. Unruh, and S.L. Jaspersen. 2016. Analysis of membrane proteins localizing to the inner nuclear envelope in living cells. *J. Cell Biol.* 215:575–590. https://doi.org/10 .1083/jcb.201607043

Stavru, F., B.B. Hülsmann, A. Spang, E. Hartmann, V.C. Cordes, and D. Görlich. 2006. NDC1: A crucial membrane-integral nucleoporin of metazoan nuclear pore complexes. *J. Cell Biol.* 173:509–519. https://doi.org/10 .1083/jcb.200601001

Strawn, L.A., T. Shen, N. Shulga, D.S. Goldfarb, and S.R. Wente. 2004. Minimal nuclear pore complexes define FG repeat domains essential for transport. *Nat. Cell Biol.* 6:197–206. https://doi.org/10.1038/ncb1097

Stukey, J.E., V.M. McDonough, and C.E. Martin. 1990. The OLE1 gene of Saccharomyces cerevisiae encodes the delta 9 fatty acid desaturase and can be functionally replaced by the rat stearoyl-CoA desaturase gene. *J. Biol. Chem.* 265:20144–20149.

Suntharalingam, M., and S.R. Wente. 2003. Peering through the pore: Nuclear pore complex structure, assembly, and function. *Dev. Cell.* 4:775–789. https://doi.org/10.1016/S1534-5807(03)00162-X

Talamas, J.A., and M.W. Hetzer. 2011. POM121 and Sun1 play a role in early steps of interphase NPC assembly. *J. Cell Biol.* 194:27–37. https://doi.org /10.1083/jcb.201012154

Tamm, T., A. Grallert, E.P. Grossman, I. Alvarez-Tabares, F.E. Stevens, and I.M. Hagan. 2011. Brr6 drives the *Schizosaccharomyces pombe* spindle pole body nuclear envelope insertion/extrusion cycle. *J. Cell Biol.* 195:467–484. https://doi.org/10.1083/jcb.201106076

Tcheperegine, S.E., M. Marelli, and R.W. Wozniak. 1999. Topology and functional domains of the yeast pore membrane protein Pom152p. *J. Biol. Chem.* 274:5252–5258. https://doi.org/10.1074/jbc.274.8.5252

Terweij, M., T. van Welsem, S. van Deventer, K.F. Verzijlbergen, V. Menendez-Benito, D. Ontoso, P. San-Segundo, J. Neefjes, and F. van Leeuwen. 2013. Recombination-induced tag exchange (RITE) cassette series to monitor protein dynamics in Saccharomyces cerevisiae. *G3 (Bethesda).* 3:1261–1272. https://doi.org/10.1534/g3.113.006213

Thiam, A.R., R.V. Farese Jr., and T.C. Walther. 2013. The biophysics and cell biology of lipid droplets. *Nat. Rev. Mol. Cell Biol.* 14:775–786. https:// doi.org/10.1038/nrm3699

Vollmer, B., M. Lorenz, D. Moreno-Andrés, M. Bodenhöfer, P. De Magistris, S.A. Astrinidis, A. Schooley, M. Flötenmeyer, S. Leptihn, and W. Antonin. 2015. Nup153 recruits the Nup107-160 complex to the inner nuclear membrane for interphasic nuclear pore complex assembly. *Dev. Cell.* 33:717–728. https://doi.org/10.1016/j.devcel.2015.04.027

Webster, B.M., P. Colombi, J. Jäger, and C.P. Lusk. 2014. Surveillance of nuclear pore complex assembly by ESCRT-III/Vps4. *Cell.* 159:388–401. https:// doi.org/10.1016/j.cell.2014.09.012

Webster, B.M., D.J. Thaller, J. Jäger, S.E. Ochmann, S. Borah, and C.P. Lusk. 2016. Chm7 and Heh1 collaborate to link nuclear pore complex quality control with nuclear envelope sealing. *EMBO J.* 35:2447–2467. https:// doi.org/10.15252/embj.201694574

Wente, S.R., and G. Blobel. 1993. A temperature-sensitive NUP116 null mutant forms a nuclear envelope seal over the yeast nuclear pore complex thereby blocking nucleocytoplasmic traffic. *J. Cell Biol.* 123:275–284. https://doi.org/10.1083/jcb.123.2.275

Wente, S.R., and M.P. Rout. 2010. The nuclear pore complex and nuclear transport. *Cold Spring Harb. Perspect. Biol.* 2:a000562. https://doi.org /10.1101/cshperspect.a000562

Winey, M., M.A. Hoyt, C. Chan, L. Goetsch, D. Botstein, and B. Byers. 1993. NDC1: A nuclear periphery component required for yeast spindle pole body duplication. *J. Cell Biol.* 122:743–751. https://doi.org/10.1083/jcb .122.4.743

Winey, M., D. Yarar, T.H. Giddings Jr., and D.N. Mastronarde. 1997. Nuclear pore complex number and distribution throughout the Saccharomyces cerevisiae cell cycle by three-dimensional reconstruction from electron micrographs of nuclear envelopes. *Mol. Biol. Cell.* 8:2119–2132. https:// doi.org/10.1091/mbc.8.11.2119

Wozniak, R.W., G. Blobel, and M.P. Rout. 1994. POM152 is an integral protein of the pore membrane domain of the yeast nuclear envelope. *J. Cell Biol.* 125:31–42. https://doi.org/10.1083/jcb.125.1.31

Yang, Y.S., and S.M. Strittmatter. 2007. The reticulons: A family of proteins with diverse functions. *Genome Biol.* 8:234. https://doi.org/10.1186/gb-2007 -8-12-234

Yang, H.J., M. Iwamoto, Y. Hiraoka, and T. Haraguchi. 2017. Function of nuclear membrane proteins in shaping the nuclear envelope integrity during closed mitosis. *J. Biochem.* 161:471–477. https://doi.org/10.1093/jb/ mvx020

Zargari, A., M. Boban, S. Heessen, C. Andréasson, J. Thyberg, and P.O. Ljungdahl. 2007. Inner nuclear membrane proteins Asi1, Asi2, and Asi3 function in concert to maintain the latent properties of transcription factors Stp1 and Stp2. *J. Biol. Chem.* 282:594–605. https://doi.org/10 .1074/jbc.M609201200